Koopman Operator Theory Applied to Lambert's Problem with a Spectral Behavior Analysis

by

Julia Pasiecznik

HBS, University of Toronto (2020)
MSc, University of Oxford (2021)

Submitted to the Department of Aeronautics and Astronautics
in partial fulfillment of the requirements for the degree of

MASTER OF SCIENCE IN AERONAUTICS AND ASTRONAUTICS

at the

MASSACHUSETTS INSTITUTE OF TECHNOLOGY

June 2023

Authored by: Julia Pasiecznik
Department of Aeronautics and Astronautics
May 23, 2023

Certified by: Richard Linares
Rockwell International Career Development Professor
Associate Professor of Aeronautics and Astronautics
Thesis Supervisor

Accepted by: Jonathan P. How
R. C. Maclaurin Professor of Aeronautics and Astronautics
Chair, Graduate Program Committee

Koopman Operator Theory Applied to Lambert's Problem with a Spectral Behavior Analysis

by

Julia Pasiecznik

Submitted to the Department of Aeronautics and Astronautics
on May 23, 2023, in partial fulfillment of the
requirements for the degree of
MASTER OF SCIENCE IN AERONAUTICS AND ASTRONAUTICS

Abstract

Astrodynamics is abundant with nonlinear dynamical systems, such as satellites operating within Earth's gravitational field. With the increase in the number of satellite constellations, making accurate predictions of the motion of satellites throughout space is becoming more relevant than ever. Influences from gravitational forces, atmospheric drag, and solar radiation pressure introduce highly nonlinear terms in the equations that model these dynamical systems. The predictions of these effects are essential for planning future space missions. Intrinsically tied to this is Lambert's problem, which concerns finding an optimal transfer orbit that connects two position vectors within a specified time of flight. Furthermore, solving Lambert's problem in the context of these nonlinear dynamical systems is crucial for identifying optimal orbit trajectories of spacecraft in Earth orbit and beyond. Traditional Lambert solvers often involve iterative methods that are computationally intensive, which may not be able to capture the nonlinearities of the dynamical systems accurately, and might have constraints in their applications. Using operator theory to simplify a system's nonlinear dynamics presents a promising avenue for research.

This Thesis bridges the gap in implementing operator theory to effectively solve Lambert's problem. The Koopman Operator is used to embed the nonlinear dynamics involved in Lambert's problem into a global linear representation, enabling the study of the nonlinear dynamical systems from a global perspective for future state prediction away from fixed points. The Koopman Operator is applied to solve variants of Lambert's problem including solving for the minimum energy and minimum Δv solutions, the single and multi-revolutions solutions, and the multi-impulse solution. Furthermore, the Koopman Operator enables the computation of these solutions with low computational complexity. A variety of initial conditions are considered, proving the range of applicability of the Koopman Operator to Lambert's problem. Comparisons made with numerical methods and another Lambert solver demonstrate the robustness and accuracy of the Koopman Operator solutions. Finally, an analysis of the spectral behaviors of the dynamics considered is provided, with insights into the stability of the dynamical systems and accuracy of the solutions found.

Thesis Supervisor: Richard Linares
Title: Rockwell International Career Development Professor
Associate Professor of Aeronautics and Astronautics

Acknowledgments

I would like to thank my advisor, Professor Richard Linares, for his support and guidance throughout my degree. I greatly appreciate his helpful insights. I would also like to thank Dr. Simone Servadio for his guidance and for our insightful discussions about Koopman Operator theory.

Thank you to my family, my parents, Sylvia and Eugene, and my twin sister Celina for their unwavering support. I also wish to thank my fellow ARClab peers, my friends, and Juanjo for all the great memories.

Contents

List of Figures

List of Tables

Chapter 1

Introduction

1.1 Motivation

The prediction of nonlinear dynamical systems in astrodynamics is an essential area of research as many problems in astrodynamics are inherently nonlinear in nature. Real-world systems often contain uncertainty in the equations of motion that describe them and in the specification of their parameters. Future state predictions are of interest to researchers who must predict the locations and velocities of celestial objects and spacecraft with high accuracy. These celestial objects and spacecraft often exist in highly nonlinear dynamical environments with influences from gravitational forces, atmospheric drag, solar radiation pressure, and electromagnetic interactions. Nonlinear dynamical systems with such influences are at the core of many astrodynamics problems including the three-body problem, the zonal harmonics problem, the prediction of the effects of nonlinear drag on satellites, and the prediction of the nonlinear effects of solar radiation pressure on spacecraft. Predicting the future states of celestial objects and spacecraft is essential for planning missions to other planets and asteroids, for tracking objects that are potential threats to Earth, and for tracking space debris in order to minimize the risk of collisions. The analysis of nonlinear dynamical systems in astrodynamics allows for improved design and optimization of space missions. Through the analysis of a nonlinear dynamical system, a researcher is better able to tune the parameters of their model for improved predictive performance

or to identify stable and unstable points. Furthermore, studying nonlinear systems in astrodynamics can help improve estimation and control of the spacecraft. This is especially important for designing low-thrust trajectories, where nonlinear optimal control plays an essential role. Moreover, analyzing nonlinear systems in astrodynamics can lead to better physical insight. Understanding the nonlinear system's governing equations of motion and stability can lead to better interpretability of the system's behavior. At the same time, it is of interest to obtain solutions to such systems quickly and reliably in many applications.

Important focus areas for future astrodynamics research have been identified to include multiple-encounter tour design, low energy trajectory design and optimization, and multiple-spacecraft trajectory optimization, among others [52]. These occur in highly nonlinear dynamical systems concerning multiple bodies and nonlinear perturbations. Furthermore, the scientific community is interested in solving trajectories to multiple small bodies such as comets or asteroids and satellite tours at outer planets [52]. These problems involve solving variants of Lambert's problem which concerns finding optimal orbit trajectories between two points in space.

A major challenge in analyzing dynamical systems in astrodynamics and solving problems such as Lambert's problem is understanding and characterizing the nonlinearities in these systems [39]. Linear systems can be easily characterized by their eigenvalues and eigenvectors and a plethora of general procedures exist for the prediction, estimation, and control of such systems. The leading perspective on studying nonlinear dynamical systems concerns the geometry of subspaces that contain local linearizations and general attractors [32]. These local linearizations are typically made around fixed points of the nonlinear dynamical system or around periodic orbits. Furthermore, global heteroclinic and homoclinic orbits connecting fixed points, periodic orbits, and different types of attractors are typically considered [60]. These linearizations allow for numerous linear analysis techniques to be applied to the study of nonlinear systems. However, the global analysis of nonlinear dynamical systems in astrodynamics has mostly been limited to numerical methods or using models that make physical approximations. Models that make physics approximations can reduce

complexity, however, they can introduce prediction error and uncertainty. Numerical solutions can also be prone to errors, be computationally expensive and time-consuming to compute. It is of interest to study these nonlinear dynamical systems from a global perspective for future state prediction, control and estimation away from fixed points and periodic orbits.

Operator theory, in particular the Koopman Operator, is a mathematical tool that can be used to project a complex dynamical system into a higher-dimensional space where the system's dynamics are simplified without making any physical approximations. Overcoming the challenges involved in solving problems in nonlinear dynamics using operator theory can transform our understanding of these complex systems and provide information on the system's behavior. The Koopman Operator is an infinite dimensional linear operator that embeds nonlinear dynamics into a global linear representation. It can be used to provide a global perspective to analyze complex dynamics efficiently and solve nonlinear problems away from fixed points. The spectral decomposition of the Koopman Operator also characterizes the nonlinear system's behavior, hence providing further insight into the stability of the nonlinear system.

1.2 General Objectives

The main objective of this Thesis is to offer insight into how operator theory, specifically Koopman Operator theory, can be applied to solve nonlinear problems in astrodynamics with a focus on solving variants of Lambert's problem. This work aims to provide a comprehensive explanation of the advantages of using operator theory to solve nonlinear problems in astrodynamics such that the key conclusions and methods can be extrapolated to other nonlinear problems in astrodynamics and beyond.

Another objective of this Thesis is to show the robustness and range of applicability of the Koopman Operator to Lambert's problem. Hence, variants of Lambert's problem are introduced and solved. In order to present the benefits of using operator theory for these types of problems, this Thesis presents a comparison to numerical integration techniques and another Lambert solver.

Finally, an objective of this Thesis is to provide a deeper understanding of the nonlinear dynamical systems in astrodynamics that are presented. Hence, a spectral behavior analysis is provided and differences between various dynamical systems are highlighted.

1.3 Literature Review

1.3.1 Koopman Operator Theory

With the development of quantum mechanics in the 1900's there came an interest in formulating classical mechanics from an operator theoretic approach. In 1931, Koopman developed the idea to use linear operators to study complex dynamical systems which became known as Koopman Operator (KO) Theory [40]. In 1932, von Neumann helped develop KO theory with his discovery of self-adjoint operators and applications of KO theory [65]. Since its invention, KO theory has been successfully applied to many nonlinear dynamics problems in astrodynamics [44], fluid dynamics [48], control theory [50], robotics [20], and machine learning among others [46]. More specifically in astrodynamics the KO has been successfully applied to solving nonlinear problems including for its use as an altitude control method [21], for describing the motion of a satellite near the L_1 and L_2 Lagrange points [44], and for the dynamics near libration points in the circular restricted three-body problem (CR3BP) [58]. In this last case, KO has shown to provide extremely accurate approximations for the solutions for small Lyapunov orbits and halo orbits. Furthermore, the KO has been successfully applied to the low-thrust trajectory optimization problem and has effectively been used to compute planar interplanetary transfers [35]. KO has also been applied to the zonal harmonics problem where errors in the position of the satellite were calculated to be in the order of magnitude of meters when compared to numerical integration of the system's equations for propagation of 360 degrees of a sun-synchronous orbit with order 7 in the KO basis functions. With an increase to order 11 in the KO basis functions this error dropped to 0.32 meters. Arnas and

Linares also showed that for long propagation times, such as 100 orbital periods, the error can increase up to the order of magnitude of kilometers [4].

Another area of research with the KO has been from a data-driven perspective. This approach uses dynamic mode decomposition (DMD) to approximate the KO with a best-fit linear model [18]. It uses data rather than prior knowledge of the dynamical system's governing equations to construct the KO and use it for an analysis of the system [62].

1.3.2 Lambert's Problem and Its Solvers

Lambert's problem concerns finding an optimal transfer orbit of an object in a gravitational inverse-square central force field given an initial and final position vector and a time of flight [12]. It is an orbital boundary value problem that has been studied by mathematicians for years and is at the core of many problems in astrodynamics. In fact, more than 60 authors have constructed various formulations and solutions to Lambert's problem to date [25]. Finding solutions to Lambert's problem is key to modern spacecraft operations such as for orbit determination, multi-planet trajectories, targeting and rendezvous. The fundamental work and formulations of Lambert's problem were developed by Euler, Lambert, Lagrange, and Gauss [16]. The problem was first researched by Euler in the mid-18th century but his developments focused on circular orbits. A general solution that accounted for elliptical orbits was then solved for by Lambert which became known as Lambert's theorem [16]. The work by Euler and Lambert was extended by Lagrange to account for hyperbolic and parabolic orbits [42]. In the early 19th century, Gauss significantly contributed to the development of Lambert's problem by advancing a numerical method that used a series of conic sections to approximate the solution [17]. Lancaster and Blanchard expanded on this work and advanced a universal form of Lambert's theorem that made use of a normalized time-of-flight equation and was valid for elliptic, hyperbolic, and parabolic orbits [12]. Gooding built upon Lancaster and Blanchard's method and developed an algorithm that solved Lambert's problem using Halley's cubic iteration method [30]. Izzo also built upon Lancaster and Blanchard's method and developed a solver with

a reduction in overall complexity [36]. Izzo's Householder algorithm has been found to have the best ratio between speed, robustness and accuracy [25]. The solutions by Lancaster and Blanchard, Gooding, and Izzo use the method of universal variables in their formulations. Other authors that have used this method in deriving their solutions to Lambert's problem include Bate, Mueller and White [8] who used the Gauss f and g functions and used Stumpff functions to express the transfer time in the form of a universal variable. Luo, Meng and Han proposed a solution algorithm that used Bate's universal variable to find Kepler orbits with a fixed flight-direction angle constraint [47]. An enhanced Lambert targeting method that uses the hodograph to calculate the velocity of the transfer for any transfer angle, including 180-degree orbital transfers, was introduced by Thompson [63]. Battin and Vaughan formulated an algorithm that was devoid of the two major flaws of Gauss' method which were that the method was singular for a transfer angle of 180 degrees and the method had a slow convergence rate for angles that were not very small [9].

Solutions to Lambert's problem that use the semi-major axis of the transfer as the free parameter include that of Thorne's solution who computed a series reversion/inversion of the time function [64]. Furthermore, Chen, Kampen and Chu used interval analysis to solve the time-open constrained Lambert problem that has the semi-major axis as the free parameter [22], while Wailliez used a simple semi-analytic inversion method [66]. Other solutions to Lambert's problem consider the semi-latus rectum of the transfer as the free parameter such as the solution proposed by Boltz that uses p-iteration [13]. Another method used to solve Lambert's problem is to use the eccentricity vector as the free parameter. Avanzini used this method to derive an algorithm that is less demanding from a mathematical standpoint and more physically intuitive than Battin's approach, although it does not provide computational advantages [6]. The analytical derivative of the transverse-eccentricity-based Lambert problem was derived by Wen, Zhao and Shi who used it to improve the algorithm introduced by Avanzini [67]. Finally, solutions to Lambert's problem using Kustaanheimo-Stiefel (K-S) regularized coordinates have also been studied by Jezewski [37] and by Kriz [41]. The use of these coordinates simplifies the problem

greatly as it involves the solution of only one nonlinear, well-behaved equation with one unknown variable. For a complete overview of approaches that have been designed to solve Lambert's problem, the reader is referred to the review by de la Torre Sangrà and Fantino [25].

An alternative to solving Lambert's problem in a chosen time interval is finding the orbit transfer that minimizes fuel consumption, also known as the minimum Δv Lambert's problem [11]. Techniques proposed to solve this problem include iterative techniques and using equations that require numerical techniques to solve [61] [55]. A closed-form solution has been found to the related minimum Δv_{tot}^2 Lambert's problem by Avendaño and Mortari [7]. The energy-optimal solution to Lambert's problem, which helps determine the most efficient path for a spacecraft, has also been explored by Leeghim and Jaroux, among others [43].

Solutions that involve multiple revolutions have been proposed using direct geometry or universal variables [5] [45] and considering various constraints [70]. A solution using the flight-path angle as the independent parameter and a novel algorithm was found by Arlulkar and Naik [1]. Shen and Tsiotras used Battin's method to obtain solutions to the multiple revolution Lambert's problem [59]. He, Li and Han built on the solution proposed by Avanzini and used the eccentricity vector of the transfer orbit to find multiple-revolution solutions [34]. Furthermore, Lambert's problem solved with multiple impulses between the initial and final orbits has been proposed by Gobetz and Doll [26], as well as by Prussing who found the minimum-fuel solution optimality of the two-impulse trajectory using primer vector theory [51].

The gravity-perturbed Lambert's problem considers the effects of zonal harmonics of the Earth in its formulation. Canonical solutions to this problem were developed by Scheifele and Graf using Delaunay similar elements that produced good numerical results [54] and by Bond who used singularity-free Pioncaré's similar elements [14]. A solution to the gravity-perturbed Lambert problem using the K-S coordinates has been proposed by Engels and Junkins [27]. Furthermore, a noncanonical analytic solution in terms of the independent variable, the true anomaly, was proposed by Jezewski [38]. Recent research developments of the J_2-perturbed Lambert's problem

have included a fast solver using a deep neural network developed by Yang, Li, Feng and Vasile [69].

1.4 Specific Objectives

As seen in the previous section, solving Lambert's problem is of interest to researchers due to its applicability to multiple space missions. However, some solvers to Lambert's problem do not take into account J_2 perturbations, do not provide analytic solutions to Lambert's problem, or are computationally expensive to employ. Designing an analytic solver that takes into account perturbations and is computationally inexpensive is a continuous research goal in the astrodynamics community. Furthermore, the results obtained so far with Koopman Operator theory applied to solving problems in astrodynamics show promise for applicability to solving Lambert's problem. However, no such application of the Koopman Operator has been made.

This Thesis focuses on the application of analytical Koopman Operator theory in order to gain approximate-analytical solutions to Lambert's problem in astrodynamics and a better understanding of the equations underlying their dynamics. Regarding this problem, the main specific objectives of this Thesis include:

1. To provide a formulation of the Koopman Operator Theory for Lambert's Problem

2. To show the wide applicability of the Koopman Operator solution by considering variants to Lambert's problem and different initial conditions

3. To compare and contrast the performance of the Koopman Operator solution to another Lambert solver and numerical integration techniques

4. To provide a deeper understanding of the nonlinear system's dynamics through a spectral behavior analysis of the Koopman Operator

The variants to Lambert's problem that are solved in this Thesis include the single revolution Lambert's problem with a minimum energy cost function, the single revolution Lambert's problem with a minimum Δv cost function, a global minimum Δv

solution given two generic orbits, the multiple revolutions Lambert's problem, and the multi-impulse solution to Lambert's problem. Furthermore, two dynamical systems are considered: that of the unperturbed dynamical system known as the two-body problem, and that of the perturbed dynamical system that takes into account J_2 effects. Throughout the Thesis comparisons between the two dynamical systems and solutions of Lambert's problem in each are made, concluding with a spectral behavior analysis of them.

1.5 Thesis Overview

This Thesis is structured as follows: Chapter 2 introduces Koopman Operator theory and provides an explanation of the computation of the Koopman eigenfunctions and evolution of the basis functions and observables of the system; Chapter 3 introduces Lambert's problem and its variants including the multiple revolution Lambert's problem, the minimum energy Lambert's problem, the minimum Δv Lambert's problem, and the multi-impulse Lambert's problem; Chapter 4 presents the results of applying the Koopman Operator to solving Lambert's problem and its variants, and discusses its performance by comparing these results to another Lambert solver and a numerical integration of the system, as well as, presents a use case for space debris; Chapter 5 provides an analysis of the spectral behavior of the solutions; finally, Chapter 6 presents a summary of the contributions and future research directions.

Chapter 2

Koopman Operator Theory

2.1 Introduction

This chapter introduces the theory behind the Koopman Operator and the mathematical methods required to apply it to nonlinear problems. Specifically, it outlines how the highly dimensional linear approximation of the nonlinear dynamical system can be achieved using the Koopman Operator.

Section 2.2 introduces the Koopman Operator and its eigenfunctions. Then Section 2.3 introduces the Galerkin method used to compute the Koopman eigenfunctions and the Koopman matrix for a given dynamical system. Finally, Section 2.4 provides the evolution of the basis functions and of the observables of the system.

2.2 Koopman Operator Formulation

The KO provides the analysis of a nonlinear system by transforming the dynamics into a global linear representation. It redefines problems in classical mechanics in operator form [4]. The KO theory introduced in this section follows the work by Servadio, Arnas and Linares [57].

Consider a classical nonlinear dynamical system represented by a coupled set of

ordinary differential equations (ODE),

$$\begin{cases} \frac{d}{dt}\mathbf{x}(t) = \mathbf{f}(\mathbf{x}) \\ \mathbf{x}\left(t_0\right) = \mathbf{x_0} \end{cases} \tag{2.1}$$

where $\mathbf{x} \in \mathbb{R}^d$ represents the state of the system and d is the dimension of the system. The state has a time dependence that expresses the evolution of the dynamical system. The nonlinear dynamics are represented by $\mathbf{f}(\mathbf{x})$ which propagates the state from the d-dimensional Euclidean space $\mathbb{R}^d$ to $\mathbb{R}^d$. The state $\mathbf{x_0}$ is the initial condition of the system at the initial time t_0. Solving for a solution of this set of ODEs is also known as an initial value problem.

The KO can be used to describe the evolution of an observable of the dynamical system over time. Conceptually, KO applies the chain rule to the observable. Let $\mathcal{K}$ denote the KO. Its application is defined as

$$\mathcal{K}(\cdot) = \left(\nabla_{\mathbf{x}} \cdot\right) \mathbf{f}(\mathbf{x}). \tag{2.2}$$

The relation can be made more explicit by considering an observable function of the dynamical system in Equation 2.1 denoted by $\boldsymbol{g}(\mathbf{x})$. The evolution of such an observable is given by

$$\begin{aligned} \mathcal{K}(\boldsymbol{g}(\mathbf{x})) &= \frac{d}{dt}\boldsymbol{g}(\mathbf{x}) \\ &= \left(\nabla_{\mathbf{x}}\boldsymbol{g}(\mathbf{x})\right) \frac{d}{dt}\mathbf{x}(t) \\ &= \left(\nabla_{\mathbf{x}}\boldsymbol{g}(\mathbf{x})\right) \mathbf{f}(\mathbf{x}) \end{aligned} \tag{2.3}$$

where $\nabla_{\mathbf{x}}\boldsymbol{g}(\mathbf{x}) = [\partial\boldsymbol{g}(\mathbf{x})/\partial x_1, \partial\boldsymbol{g}(\mathbf{x})/\partial x_2, \ldots, \partial\boldsymbol{g}(\mathbf{x})/\partial x_d]$. Let $\mathcal{G}(\mathbf{x})$ denote the set of observables where $\boldsymbol{g}(\mathbf{x}) \subseteq \mathcal{G}(\mathbf{x})$. The vector space of all observable functions, denoted by $\mathcal{F}$, where $\mathcal{G}(\mathbf{x}) \in \mathcal{F}$, is infinite dimensional as a consequence of the KO being an infinite dimensional linear operator [4]. The use of an infinite Hilbert space is impractical, hence the number of dimensions is truncated and the evolution of the dynamical system is captured in a finite-dimensional subspace. This finite subspace, $\mathcal{F}_D \in \mathcal{F}$, of dimension m, is spanned by a finite set of basis functions. This

subspace is still able to capture the non-linearities of the original system however as an approximation. Hence, the KO provides an approximate linear description of nonlinear dynamical systems, allowing for efficient computation of solutions to problems in nonlinear astrodynamical systems.

Furthermore, any set of eigenfunctions of the KO provides a Koopman invariant finite subspace $\mathcal{F}_D$. From operator theory, an eigenfunction of an operator is a function that when acted upon by the operator is simply scaled by a scalar value known as an eigenvalue [31]. Hence, eigenfunctions of the KO are defined as,

$$\mathcal{K}\left(\phi_i(\mathbf{x})\right) = \lambda_i \phi_i(\mathbf{x}) \tag{2.4}$$

where $\phi_i(\mathbf{x})$ denotes an eigenfunction and λ_i denotes the corresponding eigenvalue. Let $\mathbf{\Phi}(\mathbf{x})$ be the set of all eigenfunctions such that $\mathbf{\Phi}(\mathbf{x}) = \left(\phi_1(\mathbf{x}), \ldots, \phi_m(\mathbf{x})\right)^T \in \mathcal{F}_D$. The generalization to all eigenfunctions of Equation 2.4 is given by

$$\mathcal{K}(\mathbf{\Phi}(\mathbf{x})) = \frac{\mathrm{d}}{\mathrm{d}t}\mathbf{\Phi}(\mathbf{x}) = \mathbf{\Lambda}\mathbf{\Phi}(\mathbf{x}) \tag{2.5}$$

where $\mathbf{\Lambda}$ is a diagonal matrix containing the KO eigenvalues, $\mathbf{\Lambda} = \mathrm{diag}\left([\lambda_1, \ldots, \lambda_m]\right)$. Thus, using the KO eigenfunctions and Equation 2.5, a variable transformation, known as the Koopman Canonical Transform can be constructed to linearize the system [57]. The evolution of the eigenfunctions in time is given by the solution to equation (2.5),

$$\mathbf{\Phi}(\mathbf{x}\,(t)) = \exp(\mathbf{\Lambda}t)\mathbf{\Phi}(\mathbf{x}\,(t_0)). \tag{2.6}$$

Once the eigenfunctions of the system are found, equation (2.6) can be used to solve the complete system. This approximate linear description provided by the KO enables the utilization of many mathematical tools provided by linear algebra, such as computing the state transition matrices. However, before computing the full solution by making use of such tools, the representation of the set of eigenfunctions of the KO and the required linearization is computed using the Galerkin method.

2.3 Computation of the Koopman Eigenfunctions

The Galerkin method provides the approximated linearized system of equations needed to apply the KO theory. It projects the system onto a set of orthogonal functions that span a finite subspace of the KO theory. The method has been previously introduced by Arnas and Linares in the zonal formulation [4] . An overview of key parts of the formulation is shown here for its application to problems in nonlinear astrodynamics.

The Galerkin method converts a problem involving a continuous operator, such as the one shown in Equation 2.4, into the form of a linear combination of elements and provides a method to find its solution [28] [19]. It is a tool for finding approximate solutions to problems that involve partial differential equations. Basis functions are a set of functions that are linearly independent and can be combined to represent any function in a given functional space. Therefore, any function can be represented as a linear combination of basis functions. Orthogonal basis functions are basis functions that are orthogonal to each other. The use of orthogonal basis functions greatly simplifies computations because the coefficients of the linear combination can be computed independently. The orthogonal basis functions chosen for the proposed work are the Legendre polynomials due to their advantages in simplifying the computation of the Galerkin projections. Legendre polynomials are orthogonal polynomials that provide a complete basis. Let $\mathcal{L}(\mathbf{x})$ denote the set of all basis functions. Written in vector form, the set is given by $\mathcal{L}(\mathbf{x}) = [\mathcal{L}_1(\mathbf{x}), \ldots, \mathcal{L}_m(\mathbf{x})]^T$ where $\mathcal{L}_i(\mathbf{x})$ is a multi-dimensional basis function of the set. The orthonormal basis functions are defined using the Legendre polynomials by expressing $L_i(\mathbf{x})$ as,

$$\mathcal{L}_i(\mathbf{x}) = \prod_{j=1}^{d} P_{n_j}(\mathrm{x}_j) \tag{2.7}$$

where $P_{n_j}(\mathrm{x}_j)$ denotes the monovariable Legendre polynomial of order n_j acting on variable x_j [4]. The advantages of using Legendre polynomials over other possibilities, such as Hermite or Laguerre polynomials, include that they are defined in a bounded domain ($[-1, 1]$) and the weighting function associated with the Legendre polynomials

is a constant, $w(x) = 1$ [53].

The aim is to represent any function of the dynamical system and KO eigenfunction in terms of this set of basis functions given by the Legendre polynomials. This is done by projecting the functions onto the basis functions using the inner product,

$$\langle h(\mathbf{x}), \mathcal{L}(\mathbf{x}) \rangle = \int_{\Omega} h(\mathbf{x}) \mathcal{L}(\mathbf{x}) w(\mathbf{x}) d\mathbf{x} \tag{2.8}$$

where $h(\mathbf{x})$ is a function of the system and Ω is the domain in which the basis functions are defined in.

The KO eigenfunctions are expressed as [57],

$$\phi_i(\mathbf{x}, t) = \sum_{j=1}^{\infty} p_{ij}(t) \mathcal{L}_j(\mathbf{x}) \tag{2.9}$$

where $p_{ij}(t)$ are the coefficients of the eigenfunction $\phi_i(\mathbf{x}, t)$ in the basis $\mathcal{L}_j$. This infinite series is truncated in order to have a limited set of eigenfunctions of the system,

$$\phi_i(\mathbf{x}, t) \approx \sum_{j=1}^{m} p_{ij} \mathcal{L}_\ell(\mathbf{x}) = \mathbf{p}_i{}^T(t) \mathcal{L}(\mathbf{x}) = \mathcal{L}^T(\mathbf{x}) \mathbf{p}_i(t). \tag{2.10}$$

$\mathcal{L}$ is a column vector made up of the entire set of basis functions.

The Galerkin Method is used to compute the time derivatives of the eigenfunctions. The KO is projected into the subspace $\mathcal{F}_D$ with the residual of Equation 2.5 being orthogonal to the span of $\mathcal{F}_D$. The time evolution of a scalar function, $u(\mathbf{x}, t)$, is defined as a first-order partial differential equation (PDE) using the KO as

$$\frac{du(\mathbf{x}, t)}{dt} = f_1(\mathbf{x}) \frac{\partial}{\partial x_1} u(\mathbf{x}, t) + \cdots + f_m(\mathbf{x}) \frac{\partial}{\partial x_m} u(\mathbf{x}, t). \tag{2.11}$$

The residual error of this PDE is given by,

$$e(\mathbf{x}, t) = \frac{du(\mathbf{x}, t)}{dt} - \mathcal{K}(u(\mathbf{x}, t)) \tag{2.12}$$

However, similar to Equation 2.9, the scalar function can be written in terms of an

infinite series expansion of the set of basis functions [57],

$$u(\mathbf{x},t) = \sum_{j=1}^{\infty} c_j(t)\mathcal{L}_j(\mathbf{x}) \tag{2.13}$$

where the coefficients $c_j(t)$ provide the time evolution of $u(\mathbf{x},t)$. This infinite series is also truncated in order,

$$u(\mathbf{x},t) \approx \sum_{j=1}^{m} c_j\mathcal{L}_j(\mathbf{x}) = \mathbf{c}^T(t)\mathcal{L}(\mathbf{x}) = \mathcal{L}^T(\mathbf{x})\mathbf{c}(t) \tag{2.14}$$

Hence, the derivative of $u(\mathbf{x},t)$ in the residual in Equation 2.12 can be approximated as, $\dot{u}(\mathbf{x},t) \approx \dot{\mathbf{c}}^T(t)\mathcal{L}$. The KO applied to the scalar function is given by,

$$\begin{aligned}
\mathcal{K}(u(\mathbf{x},t)) &= \frac{d}{dt}u(\mathbf{x},t) \\
&= \frac{d}{dt}(\mathcal{L}^T(\mathbf{x})\mathbf{c}(t)) \\
&= (\nabla_{\mathbf{x}}(\mathcal{L}^T(\mathbf{x})\mathbf{c}(t)))^T\frac{d}{dt}\mathbf{x}(t) \\
&= (\nabla_{\mathbf{x}}\mathcal{L}^T(\mathbf{x})\mathbf{c}(t))^T\mathbf{f}(\mathbf{x}) \\
&= \mathbf{f}^T(\mathbf{x})\nabla_{\mathbf{x}}\mathcal{L}^T(\mathbf{x})\mathbf{c}(t)
\end{aligned} \tag{2.15}$$

Since $\mathcal{L}_j(\mathbf{x})$ is defined in $\mathcal{F}_D$, for the residual to be defined in a space orthogonal to $\mathcal{F}_D$, the following relation must hold,

$$\langle \mathcal{L}_j(\mathbf{x}), e(\mathbf{x},t)\rangle = 0, \quad \forall j \in \{1,2,\ldots,m\}. \tag{2.16}$$

Substituting Equation 2.15 and Equation 2.14 into Equation 2.16 for each basis function, the matrix representation of the KO over the basis functions is derived [57],

$$\mathbf{K}_{ij} = \left\langle \mathcal{L}_i(\mathbf{x}), \mathbf{f}^T\nabla_{\mathbf{x}}\mathcal{L}_j(\mathbf{x})\right\rangle \tag{2.17}$$

where the orthogonality of the basis functions was used to simplify the equations. These are the components of the Koopman matrix.

2.4 Evolution of Basis Functions

To use the Koopman approach and the fact that the orthogonal basis functions are selected to be defined in terms of the Legendre polynomials, it is of interest to express their change over time in terms of themselves,

$$\frac{d\mathcal{L}}{dt} = \tilde{\mathbf{K}}\mathcal{L} \tag{2.18}$$

where $\tilde{\mathbf{K}}$ is the transpose of the Koopman matrix from Equation 2.17. This formulation describes how the system evolves over time [57]. The rate of change in Equation 2.18 is defined in terms of a linear combination of the Legendre polynomials with an exact solution attainable in an infinite dimensional Hilbert space. When truncating this solution to a finite dimensional space, the higher the order of the KO used, the more eigenfunctions are used. The greater the number of eigenfunctions used, the better the nonlinearities of the system are captured and hence a more accurate solution is found. This increase in the number of eigenfunctions used comes at a cost of increasing the size of the KO matrix. However, the KO matrix only needs to be calculated once for the dynamical system and can then be applied to any initial conditions.

The observables must now be represented as a linear combination of the system's basis functions. To achieve this, the projection of the observables onto the basis functions is calculated using the inner product. Using the jth basis function, the projection is calculated as [57],

$$\boldsymbol{g} = \sum_{j=0}^{m} \langle \boldsymbol{g}, \mathcal{L}_j \rangle \, \mathcal{L}_j. \tag{2.19}$$

In matrix form, the set of coefficients that expresses the projection of the ith observable onto the jth basis function is given as,

$$\mathcal{H}_{ij} = \langle g_i, \mathcal{L}_j \rangle \tag{2.20}$$

Furthermore, finding the eigendecomposition of the system is of interest in order to eventually calculate the time evolution of the observables. Let V represent the matrix of eigenvectors and Λ represent the diagonal matrix of the eigenvalues. Assuming the Koopman matrix is diagonalizable, the eigendecomposition of the system is given by,

$$V\mathbf{K} = \Lambda V. \tag{2.21}$$

If the Koopman matrix is not diagonalizable then further steps must be taken using the Schur decomposition as described by Arnas in [2]. Using the eigendecomposition, the eigenfunctions can be written in terms of the eigenvectors and Legendre polynomials as,

$$\phi(\mathbf{x}(t)) = V\mathcal{L}(\mathbf{x}(t)) \tag{2.22}$$

with the rate of change of the eigenfunctions given by,

$$\begin{aligned} \frac{d}{dt}\phi(\mathbf{x}(t)) &= \frac{d}{dt}(V\mathcal{L}(\mathbf{x}(t))) \\ &= V\mathbf{K}\mathcal{L}(\mathbf{x}(t)) \\ &= \Lambda V\mathcal{L}(\mathbf{x}(t)) \\ &= \Lambda\phi(\mathbf{x}(t)) \end{aligned} \tag{2.23}$$

where the fact that V is constant was used to take it out of the derivative and substitutions using Equations 2.18, 2.21, and 2.22 were made. The solution to this diagonal system of ODEs is,

$$\phi(\mathbf{x}(t)) = \exp(\Lambda t)\phi\left(\mathbf{x}\left(t_0\right)\right) \tag{2.24}$$

where $\phi\left(\mathbf{x}\left(t_0\right)\right)$ represents the initial value of the eigenfunctions at the initial time t_0. Using the matrix $\mathcal{H}$ from Equation 2.20 and the representation of the eigenfunctions

in Equation 2.22, the evolution of the observables in time is given by [57],

$$\begin{aligned} \boldsymbol{g}(\mathbf{x}(t)) &= \mathcal{H}\mathcal{L}(\mathbf{x}(t)) \\ &= \mathcal{H}V^{-1}\phi(\mathbf{x}(t)) \\ &= \mathcal{H}V^{-1}\exp(\Lambda t)\phi\left(\mathbf{x}\left(t_0\right)\right) \\ &= \mathcal{H}V^{-1}\exp(\Lambda t)V\mathcal{L}\left(\mathbf{x}\left(t_0\right)\right). \end{aligned} \tag{2.25}$$

where a substitution using Equation 2.24 was made at the third step and a substitution using Equation 2.22 was made at the last step. Hence, through the evolution of the observables, the evolution of the state of the system can be calculated in terms of the evolution of the eigenfunctions by selecting the identity observable. For any time, t, the value of an observable can now be calculated. Furthermore, the matrix $\mathcal{H}$ is the only term that is dependent upon the selection of the observable. Hence, once the Koopman matrix $\mathbf{K}$ is calculated, the time evolutions of new observables of the system are evaluated by recalculating $\mathcal{H}$. Since, the ability to understand and predict the behavior of a system comes from its observables, their time evolution are of primary interest to compute. In conclusion, the computation of the time evolution of observables using the Koopman matrix and $\mathcal{H}$ allows for the propagation of the state of the system.

Chapter 3

Lambert's Problem and Algorithm Implementations

3.1 Introduction

The formulation of Lambert's problem is presented in this Chapter, as well as variants of it that will be solved in the remaining Chapters of the Thesis. Furthermore, key algorithms that will be used either for comparison or within the KO Lambert solver are introduced.

To that end, Section 3.2 sets up the details of Lambert's problem. Then, Section 3.3 introduces the Lambert solver that uses Lagrange coefficients and will be used to compare against the solutions found using the Koopman Operator. Section 3.4 introduces the algorithm used as part of the Koopman Operator solution to Lambert's problem. Finally, Section 3.5 introduces the elements used in the Koopman Operator formulation of Lambert's problem.

3.2 Overview of Lambert's Problem

Lambert's problem concerns the determination of an optimal transfer orbit between a specified initial and final position vector and a time of flight. A depiction of the problem is shown in Figure 3-1, where $\mathbf{r}_0$ is the initial position vector, $\mathbf{r}_f$ is the final

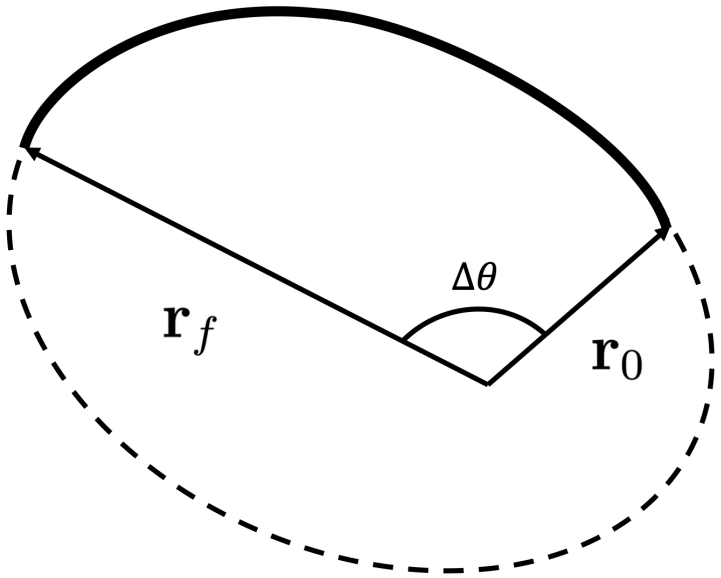

Figure 3-1: Geometry of Lambert's problem

position vector and a transfer orbit connects the two. $\Delta\theta$ is the change in true anomaly between the two vectors. The geometric approach to solving Lambert's problem involves determining the semimajor axis of the transfer orbit using the chord length, or the shortest distance between two position vectors. Two possible transfers exist, one called the "short way" which follows the solid line in Figure 3-1 and one called the "long way" which follows the dashed line. When considering the problem in the context of transfers around the Earth or another spinning body, the two possible transfers are more generally defined as "prograde" which involves the spacecraft moving in the same direction as the planet's rotation and "retrograde" which involves the spacecraft moving in the opposite direction to the planet's rotation. Prograde solutions are typically preferred for missions such as geostationary orbit insertion as they require less Δv. However, retrograde solutions may be used for missions involving Sun-synchronous or polar orbits.

In this Thesis, Lambert's problem is solved using a geometric approach using the KO theory. Solutions are presented to Lambert's problem within two systems, one that does not take into account the oblateness of the Earth and one that takes into

account the oblateness. In the first case, the dynamics assume a spherical central body around which a satellite travels. In the second case, the dynamics take into account J_2 effects and hence reduce inaccuracies in the trajectory of a spacecraft in Earth's gravitational field.

A variant of Lambert's problem is the multiple-revolutions Lambert's problem which concerns finding transfer orbits that complete a number of revolutions between the initial and final position vector. Solving the multiple-revolutions Lambert's problem allows for more complex orbital maneuvers of spacecraft to be executed including transfer trajectories between planets and for finding transfers that require less Δv than a single revolution transfer. Multiple revolution solutions add flexibility to space missions. They can provide more efficient transfers when compared to direct transfers by taking advantage of the gravitational fields of celestial bodies. The solutions can involve a series of "swing-bys" to achieve a desired trajectory using less propellant than a direct transfer would. Such multiple revolution solutions are typically desirable for long-range space missions such as for the European Space Agency's BepiColombo mission to Mercury which performed a gravity assist with Earth in April 2020 and will perform several more with Venus and Mercury during the mission [10]. An example of a multi-revolution solution with only one revolution is traversing the solid black line from $\mathbf{r}_0$ to $\mathbf{r}_f$ in Figure 3-1, followed by the dashed line and finally once more traversing the solid line before reaching $\mathbf{r}_f$.

The multi-impulse solution to Lambert's problem involves a series of small burns at specific points in the orbit transfer rather than a single large burn corresponding to one impulse. An example of a multi-impulse trajectory with n impulses is shown in Figure 3-2. An impulse is carried out at each $\mathbf{r}_i$ for $i = 0, \ldots, n-1$ connecting $\mathbf{r}_0$ to $\mathbf{r}_f$. These multiple impulses allow for more precise control over the spacecraft's trajectory. Furthermore, they can help minimize the fuel requirements which can be essential for designing efficient and effective space missions.

Variants of Lambert's problem concern minimizing different cost functions for the transfer orbit rather than fixing a time of flight. These cost functions include specific energy, Δv, and time. The minimum energy Lambert's problem concerns finding the

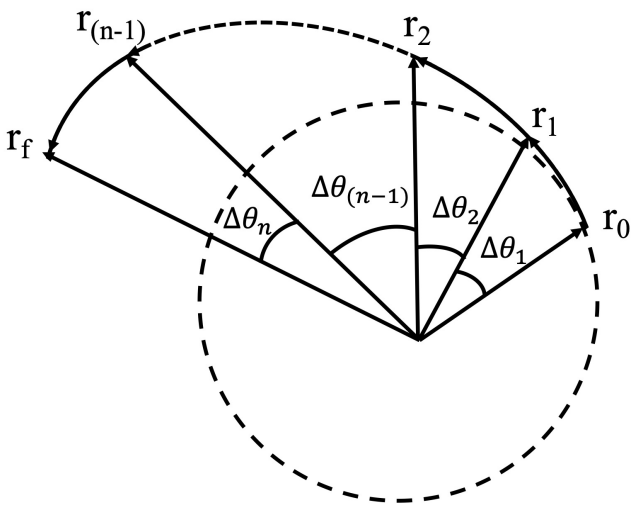

Figure 3-2: Geometry of the Multi-Impulse Solution to Lambert's Problem

transfer orbit with the minimum specific energy. It is of interest to space missions such as long-duration missions and interplanetary travel missions to find such transfer orbits as these missions require energy conservation. The minimum Δv Lambert's problem concerns finding the orbit transfer that minimizes the total change in velocity from the initial orbit to the transfer orbit and from the transfer orbit to the final orbit. Solving the minimum Δv solution is important for spacecraft operations as it reduces the total fuel consumption and cost of the mission. Finally, solving the minimum time Lambert's problem is of use for time-critical missions including satellite launches and manned missions where short orbit transfers are desirable.

3.3 Algorithm to Solve Lambert's Problem using Lagrange Coefficients

The algorithm used to compare against the solutions found by applying the KO to solving Lambert's problem is presented in this section. This algorithm makes use of Lagrange coefficients and follows the procedure presented by Bate, Mueller and White [8] and Bond and Allman [15].

A general outline of the algorithm, as described in Chapter 5.3 of the Orbital Mechanics for Engineering Students textbook by H. Curtis [24], is provided in this section. The initial position vector of a desired transfer is denoted as $\mathbf{r}_0$, and the final position vector as $\mathbf{r}_f$ with a time of flight denoted by Δt. The trajectory connecting $\mathbf{r}_0$ to $\mathbf{r}_f$ can be either a prograde or retrograde trajectory. The change in true anomaly in either case is calculated using:
For a prograde trajectory:

$$\Delta\theta = \begin{cases} \cos^{-1}\left(\dfrac{\mathbf{r}_0 \cdot \mathbf{r}_f}{r_0 r_f}\right) \text{ if } (\mathbf{r}_0 \times \mathbf{r}_f)_Z \geq 0 \\ 360^\circ - \cos^{-1}\left(\dfrac{\mathbf{r}_0 \cdot \mathbf{r}_f}{r_0 r_f}\right) \text{ if } (\mathbf{r}_0 \times \mathbf{r}_f)_Z < 0 \end{cases} \tag{3.1}$$

For a retrograde trajectory:

$$\Delta\theta = \begin{cases} \cos^{-1}\left(\dfrac{\mathbf{r}_0 \cdot \mathbf{r}_f}{r_0 r_f}\right) \text{ if } (\mathbf{r}_0 \times \mathbf{r}_f)_Z < 0 \\ 360^\circ - \cos^{-1}\left(\dfrac{\mathbf{r}_0 \cdot \mathbf{r}_f}{r_0 r_f}\right) \text{ if } (\mathbf{r}_0 \times \mathbf{r}_f)_Z \geq 0 \end{cases} \tag{3.2}$$

The Lagrange coefficients, $f, g, \dot{f}, \dot{g}$, that relate the initial position and velocity vectors to the final position and velocity vectors,

$$\begin{aligned} \mathbf{r}_f &= f\mathbf{r}_0 + g\mathbf{v}_0 \\ \mathbf{v}_f &= \dot{f}\mathbf{r}_0 + \dot{g}\mathbf{v}_0 \end{aligned} \tag{3.3}$$

are given by,

$$\begin{aligned} f &= 1 - \frac{\mu r_2}{h^2}(1 - \cos\Delta\theta) \\ g &= \frac{r_1 r_2}{h}\sin\Delta\theta \\ \dot{f} &= \frac{\mu}{h}\frac{1-\cos\Delta\theta}{\sin\Delta\theta}\left[\frac{\mu}{h^2}(1-\cos\Delta\theta) - \frac{1}{r_1} - \frac{1}{r_2}\right] \\ \dot{g} &= 1 - \frac{\mu r_1}{h^2}(1 - \cos\Delta\theta) \end{aligned} \tag{3.4}$$

where h is the unknown angular momentum. Some details in the last step are omitted for brevity. These include the use of an iterative Newton solver and Stumpff functions

to solve for analytic expressions for $f, g, \dot{f}$, and $\dot{g}$. Once these expressions are found, $\mathbf{v}_0$ can be solved for using Equation 3.3 and hence the optimal orbit trajectory connecting $\mathbf{r}_0$ and $\mathbf{r}_f$ is found. It is important to note that this algorithm does not consider the effects of zonal perturbations due to Earth's oblateness in its solution to Lambert's problem.

3.4 Levenberg-Marquadt Algorithm

The Levenberg-Marquadt algorithm will be used to solve for the initial velocity of the optimal orbit trajectory in the KO solution to Lambert's problem. The Levenberg-Marquadt algorithm is a numerical optimization method used to solve non-linear least squares problems. It is used to find the minimum of a function, $F(x)$, that is a sum of squares of nonlinear functions, $f_i(x)$,

$$F(x) = \frac{1}{2}\sum_{i=1}^{m} f_i(x)^2. \tag{3.5}$$

It searches in the direction given by the solution to the equations,

$$\left(J_k^T J_k + \lambda_k I\right) p_k = -J_k^T f_k \tag{3.6}$$

where $J_i(x)$ denotes the Jacobian of the ith function, $f_i(x)$, I is the identity matrix, λ_k are nonnegative scalars, and a unit step is taken along p_k. The vector p_k is the solution of the constrained problem,

$$\begin{aligned} \underset{p\in\mathbb{R}^n}{\text{minimize}} \quad & \tfrac{1}{2}\left\|J_k p + f_k\right\|_2^2 \\ \text{subject to} \quad & \|p\|_2 \leq \Delta \end{aligned} \tag{3.7}$$

where Δ represents a scalar, the value of which is associated with the value of λ [29].

3.5 Orbital Elements for Koopman Operator Approach

For an efficient application of the KO to a nonlinear system, such as in Lambert's problem, the system must exhibit linear-like behavior with minor perturbations. Such a system enables the limited number of basis functions to capture the non-linearities of the system, as well as, for the KO theory to efficiently find the solution to the nonlinear astrodynamical problem. This section presents the orbital elements used to represent both the unperturbed and perturbed dynamical systems so that KO can be applied to solve Lambert's problem.

Let r represent the radial distance between the orbiting satellite and the center of the Earth, φ represent the latitude of the satellite, and λ represent the longitude of the satellite. The conjugate momenta of the system are given by

$$\begin{aligned} p_r &= \dot{r} \\ p_\varphi &= r^2\dot{\varphi} \\ p_\lambda &= r^2\cos^2(\varphi)\dot{\lambda} \end{aligned} \tag{3.8}$$

where $\dot{x}$ is the derivative of the variable x with respect to time. The Hamiltonian of such a system in spherical coordinates is,

$$\mathcal{H} = \frac{1}{2}\left(p_r^2 + \frac{p_\varphi^2}{r^2} + \frac{p_\lambda^2}{r^2\cos^2(\varphi)}\right) - \frac{\mu}{r} + \frac{1}{2}\mu R_\oplus^2 J_2 \frac{1}{r^3}\left(3\sin^2(\varphi) - 1\right) \tag{3.9}$$

where μ represents the gravitational constant of the Earth, $R_\oplus$ represents the Earth's equatorial radius, and J_2 is the zonal term of the Earth's gravitational potential. The

associated equations of motion in Cartesian coordinates are,

$$
\begin{aligned}
\frac{dx}{dt} &= \dot{x} \\
\frac{dy}{dt} &= \dot{y} \\
\frac{dz}{dt} &= \dot{z} \\
\frac{d\dot{x}}{dt} &= \frac{3J_2R_e^2\mu x z^2}{(x^2+y^2+z^2)^{7/2}} - \frac{\mu x}{(x^2+y^2+z^2)^{3/2}} \\
&\quad + \frac{9J_2R_e^2\mu x}{2(x^2+y^2+z^2)^{5/2}}\left(\frac{z^2}{x^2+y^2+z^2} - \frac{1}{3}\right) \\
\frac{d\dot{y}}{dt} &= \frac{3J_2R_e^2\mu y z^2}{(x^2+y^2+z^2)^{7/2}} - \frac{\mu y}{(x^2+y^2+z^2)^{3/2}} \\
&\quad + \frac{9J_2R_e^2\mu y}{2(x^2+y^2+z^2)^{5/2}}\left(\frac{z^2}{x^2+y^2+z^2} - \frac{1}{3}\right) \\
\frac{d\dot{z}}{dt} &= -\frac{3J_2R_e^2\mu z}{2(x^2+y^2+z^2)^{3/2}}\left(\frac{2}{(x^2+y^2+z^2)} - \frac{2z^2}{(x^2+y^2+z^2)^2}\right) \\
&\quad - \frac{\mu z}{(x^2+y^2+z^2)^{3/2}} + \frac{9J_2R_e^2\mu z}{2(x^2+y^2+z^2)^{5/2}}\left(\frac{z^2}{x^2+y^2+z^2} - \frac{1}{3}\right)
\end{aligned}
\tag{3.10}
$$

These equations are highly non-linear and hence a transformation of variables is required in order to apply the KO. Such a transformation has been defined by Arnas and Linares [4], and the new set of orbital elements describing the nonlinear system

in terms of r, φ, λ, and the conjugate momenta are,

$$\begin{aligned}
\Lambda &= \sqrt{\frac{R_\oplus}{\mu}}\left(\frac{p_\theta}{r} - \frac{\mu}{p_\theta}\right) \\
\eta &= p_r\sqrt{\frac{R_\oplus}{\mu}} \\
s &= \sin(\varphi) \\
\gamma &= \frac{p_\varphi}{p_\theta}\cos(\varphi) \\
\kappa &= \sqrt{\frac{\mu R_\oplus}{p_\varphi^2 + \frac{p_\lambda^2}{\cos^2(\varphi)}}} \\
\beta &= \lambda - \arcsin\left(\tan(\varphi)\sqrt{\frac{p_\lambda^2}{p_\theta^2 - p_\lambda^2}}\right) \\
\chi &= \frac{p_\lambda}{p_\theta^4}\frac{\left(\mu R_\oplus\right)^{3/2}}{\sin^2(\varphi) + \frac{p_\varphi^2}{p_\theta^2}\cos^2(\varphi)} \\
\rho &= \frac{p_\lambda}{p_\theta}
\end{aligned} \tag{3.11}$$

where

$$p_\theta = \sqrt{p_\varphi^2 + \frac{p_\lambda^2}{\cos^2(\varphi)}} \tag{3.12}$$

is the angular momentum of the orbit. This set of orbital elements are normalized.

The corresponding Hamilton equations given in the set of new orbital elements are

$$\begin{aligned}
\frac{d\Lambda}{d\theta} &= -\eta - 3J_2 s\gamma\kappa^3(\Lambda+\kappa)(\Lambda+2\kappa) \\
\frac{d\eta}{d\theta} &= \Lambda + \frac{3}{2}J_2\kappa^3(\Lambda+\kappa)^2\left(3s^2-1\right) \\
\frac{ds}{d\theta} &= \gamma \\
\frac{d\gamma}{d\theta} &= -s - 3J_2 s\rho^2\kappa^3(\Lambda+\kappa) \\
\frac{d\kappa}{d\theta} &= 3J_2 s\gamma\kappa^4(\Lambda+\kappa) \\
\frac{d\beta}{d\theta} &= -3J_2 s^2\chi(\Lambda+\kappa) \\
\frac{d\chi}{d\theta} &= 12J_2 s\gamma\chi\kappa^3(\Lambda+\kappa) + 6J_2 s\rho\chi^2(\Lambda+\kappa) \\
\frac{d\rho}{d\theta} &= 3J_2 s\gamma\rho\kappa^3(\Lambda+\kappa)
\end{aligned} \tag{3.13}$$

This set of equations is polynomial and close to linear with nonlinear perturbations due to zonal effects. They have been defined in terms of a time regularization proposed by Arnas and Linares [3],

$$\frac{d\theta}{dt} = \frac{p_\theta}{r^2}. \tag{3.14}$$

For a detailed derivation of these orbital elements, the reader is referred to the zonal formulation made by Arnas and Linares in [4].

The linear system defined by the linear contributions to the elements in Equation 3.13 that do not have any terms proportional to J_2 give the system of Hamilton equations for the classical two body problem without J_2 effects,

$$\begin{aligned}
\frac{d\Lambda}{d\theta} &= -\eta \\
\frac{d\eta}{d\theta} &= \Lambda \\
\frac{ds}{d\theta} &= \gamma \\
\frac{d\gamma}{d\theta} &= -s \\
\frac{d\kappa}{d\theta} &= 0 \\
\frac{d\beta}{d\theta} &= 0 \\
\frac{d\chi}{d\theta} &= 0 \\
\frac{d\rho}{d\theta} &= 0
\end{aligned} \tag{3.15}$$

The Hamilton equations in Equation 3.15 and Equation 3.13 are the observables $\boldsymbol{g}(\mathbf{x})$ from Section 2.2 of the nonlinear system whose evolution is given by applying the KO.

The formulation of Lambert's problem considered in this Thesis is mostly posed in terms of having time as a constraint rather than θ. Hence, the integration of Equation 3.14 is used to convert from time to θ. This conversion allows for the use of Equation 3.13 and Equation 3.15, which are defined in terms of θ, to represent the respective dynamical system while solving a time-constrained nonlinear problem. An example comparing the propagation of time and that of the time regularization derived from Equation 3.14 with respect to θ, for one revolution of a random orbit, is shown in Figure A-1 in Appendix A. The figure shows how the regularized time is not linear in θ by demonstrating how the spacecraft slows down and accelerates depending on its location. Finally, most problems in astrodynamics are formulated in Cartesian, Spherical or Keplerian coordinates. Hence, to make use of the orbital elements in Equation 3.11, a transformation of variables is made. Once the solution is found

using the KO in terms of these new orbital elements, the inverse transformations are used to transform back to familiar coordinates.

Chapter 4

Koopman Operator Theory Applied to Solving Lambert's Problem

4.1 Introduction

This chapter applies the theory from Chapter 2 to solving Lambert's problem as formulated in Chapter 3. Various initial conditions are considered and solutions to variants of Lambert's problem are presented.

First, Section 4.2 introduces the single revolution solution to Lambert's problem solved using the Koopman Operator for both the unperturbed and perturbed dynamical systems. In Section 4.3 the solutions obtained using the Koopman Operator are compared with those found using the solver based on Lagrange coefficients, as introduced in Chapter 3. Next, the range of applicability of the Koopman Operator solution is displayed through it applications to a variety of initial conditions in Section 4.4. Section 4.5 presents the minimum energy and minimum Δv solutions to Lambert's problem using the Koopman Operator. Section 4.6 presents the Koopman Operator multiple revolutions solution to Lambert's problem. In Section 4.7, a method is presented for error-correcting the Koopman Operator transfer orbit solution. Section 4.8 presents a multi-impulse solution to Lambert's problem. Finally, Section 4.9 shows a use case of the Koopman Operator solution to Lambert's problem applied to an explosion of space debris.

4.2 Lambert's Problem Single Revolution

The solution to the single-revolution Lambert's problem concerns finding an optimal transfer orbit from an initial position vector to a final position vector within a specified time of flight. First, the solutions for the dynamics of the unperturbed system that does not take into account J_2 effects are presented, followed by the solutions for the perturbed system.

Many different initial and final conditions are considered in this chapter in Cartesian, Spherical, and Keplerian coordinates. The solutions to Lambert's problem for these various conditions do not require a recalculation of the KO matrix. Hence, the process of finding the solution is broken down into these steps,

1. Calculate the KO matrix for the dynamics of the system in consideration and for the chosen order of the basis functions

2. Pass in the set of initial conditions to the polynomial map created by the KO that directly connects the initial state to the final state

3. Use the Levenberg-Marquadt algorithm to pass in different time constraints and find the corresponding optimal orbital trajectories

4. If making use of a cost function, calculate the corresponding quantity for each of the optimal orbital trajectories and identify the trajectory which minimizes the cost function

Apply the cost function to each potential optimal orbital trajectory, calculate their corresponding values, and identify the trajectory with the minimum cost as the most efficient path.

In this Thesis, the first step is completed once for the dynamics of the unperturbed system and once for the dynamics of the perturbed system for each chosen order of the basis functions. In general, the KO matrix needs to be recalculated only when the dynamics of the system in consideration is altered such as in the case of including J_2 perturbations or other perturbations that are not considered in this Thesis such as atmospheric drag.

4.2.1 Unperturbed System

The unperturbed system dynamics are modeled using the Hamilton equations in Equation 3.15. The initial conditions from Example 5.2 of the Orbital Mechanics for Engineering Students textbook by H. Curtis are considered [24]. The initial and final position vectors are,

$$\begin{aligned} \mathbf{r}_0 &= [5000,\ \ 10,000,\ \ 2100] \text{ km} \\ \mathbf{r}_f &= [-14,600,\ \ 2500,\ \ 7000] \text{ km} \end{aligned} \tag{4.1}$$

The time of flight is 3600 seconds. The central angle between the initial and final position vectors, $\Delta\theta$, is given by:

$$\Delta\theta = \arccos \frac{\mathbf{r}_0 \cdot \mathbf{r}_f}{|\mathbf{r}_0||\mathbf{r}_f|}, \tag{4.2}$$

$\Delta\theta$ is also known as the true anomaly deviation. The required initial velocity for such a transfer orbit is solved using the Levenberg-Marquardt algorithm (LM) described in Section 3.4. An initial circular velocity guess is passed into the LM algorithm. The initial velocity guess is then passed through the KO solution in Equation 2.25 and the final position and time are found for such initial conditions. The order of the basis functions of the KO is chosen as 3 since the system is simple with no more than 2 variables in each equation and no powers greater than 1. The LM algorithm changes the initial velocity guess with each iteration through the KO matrix with the objective of minimizing the difference,

$$\Delta = [r_{f_x}, r_{f_y}, r_{f_z}, t_f] - [r_{a_x}, r_{a_y}, r_{a_z}, t_a] \tag{4.3}$$

where $[\mathbf{r}_f, t_f]$ represents the desired final position and specified time of flight and $[\mathbf{r}_a, t_a]$ represents the attained final position and time of flight. The attained time of flight is calculated using Equation 3.14. The resulting orbital trajectory is plotted in Figure 4-1. Passing in different initial conditions does not require recalculating the KO matrix as the KO matrix is calculated only once by projecting the dynamics of the system onto the basis functions. Hence, the orbital trajectories for different times can

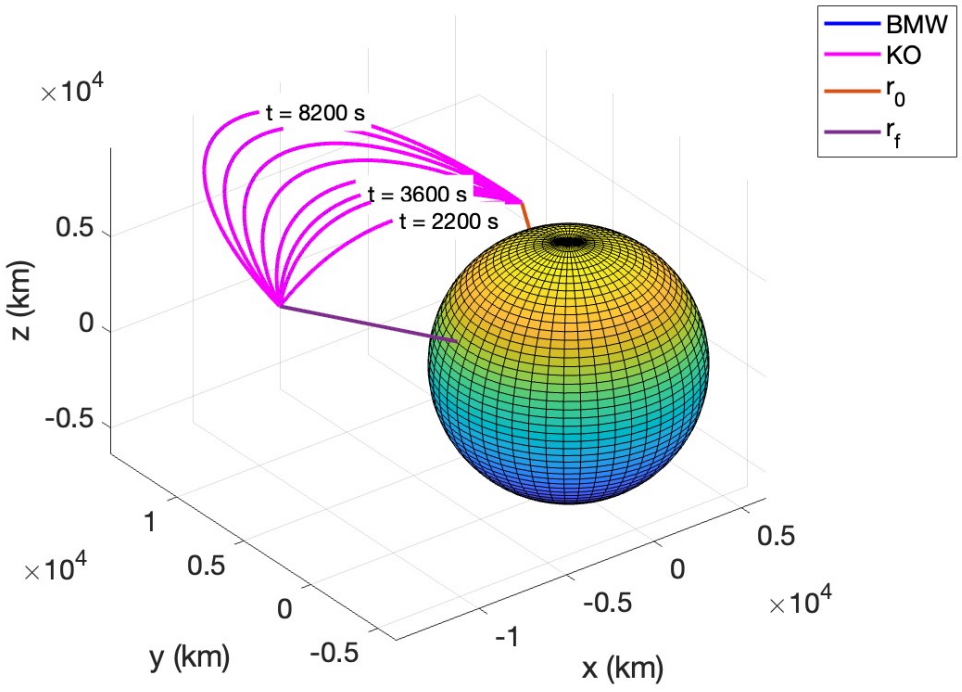

Figure 4-1: Single Revolution Optimal Trajectories without J_2 Effects

easily be calculated. The resulting trajectories for seven different times equally spaced between 1200s and 8200s are shown in Figure 4-1. The two body problem solved using the algorithm by Bate, Mueller and White and Bond and Allman (labeled as BMW in the Figures), as introduced in Section 3.3, is plotted for comparison. The two types of solutions closely overlap.

4.2.2 Perturbed System

Perturbations due to the oblateness of the Earth are taken into account by including the J_2 terms in the Hamilton equations (3.13). In order to calculate the optimal trajectories, the order of the basis functions of the KO is increased up to order 7. The maximum order of the monomials in the perturbed dynamical system is 7, hence having order 7 of the Legendre polynomials guarantees to cover any nonlinear contributions. Increasing the order improves the accuracy of the solution by being

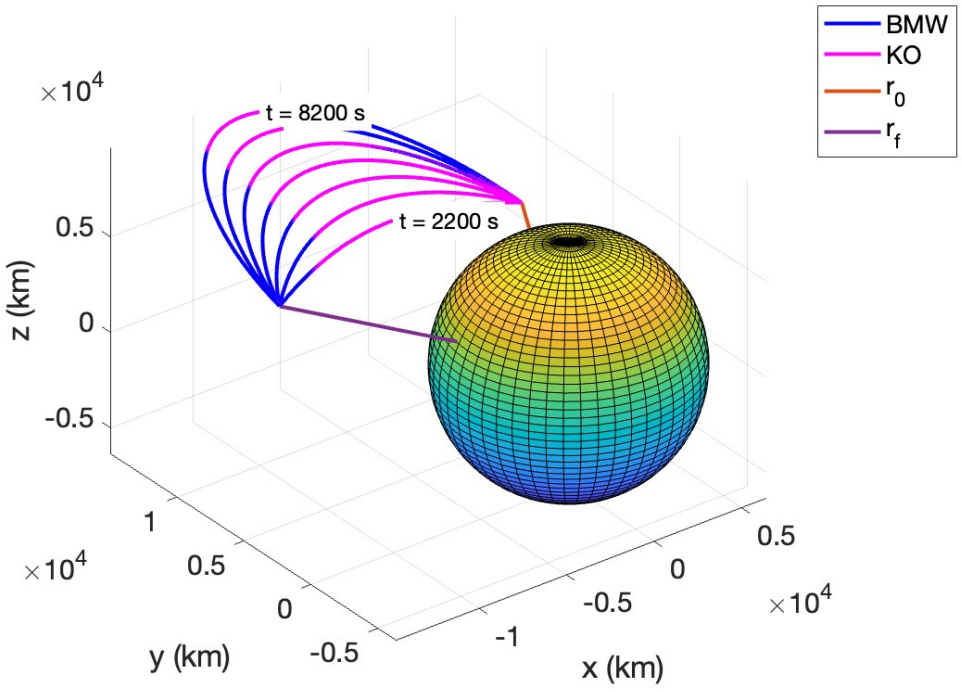

Figure 4-2: Single Revolution Optimal Trajectories with J_2 Effects

able to better take into account the non-linearities of the system. The resulting orbital trajectories found for the same seven different times as in the unperturbed case, between 1200s and 8200s, are plotted in Figure 4-2.

4.3 Error Performance

The accuracy of the solutions found using the KO Lambert solver is demonstrated by two comparisons. The first comparison is to the solutions found using the Lambert solver algorithm by Bate, Mueller and White, and Bond and Allman. The second comparison is the propagation of the solution using the KO to the propagation of the solution using a Runge-Kutta scheme of order 4-5.

The initial conditions from Section 4.2.1 are considered. The solutions found for the unperturbed system in Section 4.2.1 and for the perturbed system in Section 4.2.2 using KO are compared to the solutions found using the BMW algorithm. First, the

initial velocities found using both BMW, $\mathbf{BMW_v}$, and KO, $\mathbf{KO_{vnoJ}}$, that give the transfer orbits for the single revolution case without taking into account J_2 effects for the time constraint of $t = 3600$s are propagated. Then the initial velocity found using KO taking into account $J2$ effects, $\mathbf{KO_{vJ}}$, is propagated. These velocities and the norm of their difference is,

$$\begin{aligned}
\mathbf{KO_{vnoJ}} &= [-5.99249617,\ \ 1.92536583,\ \ 3.24563815] \text{ km/s} \\
\mathbf{KO_{vJ}} &= [-5.99201592,\ \ 1.92541067,\ \ 3.24800712] \text{ km/s} \\
\mathbf{BMW_v} &= [-5.99249502,\ \ 1.92536671,\ \ 3.24563805] \text{ km/s} \\
|\mathbf{KO_{vnoJ}} - \mathbf{BMW_v}| &= 1.458 \text{ x } 10^{-6} \text{ km/s} \\
|\mathbf{KO_{vJ}} - \mathbf{BMW_v}| &= 0.002417 \text{ km/s}
\end{aligned} \tag{4.4}$$

The propagator takes the initial state of the system and propagates it for the time of flight to find the final state in order to validate results. The propagation is first done in a two-body system without J_2 effects using a Runge-Kutta scheme of order 4-5. The norm of the difference between the final position that the satellite reaches and the desired final position, $\mathbf{r}_f$, is 2.543×10^{-10} km for the velocity found using the Lambert solver by BMW, $\mathbf{BMW_v}$, and 0.00421 km for the velocity found using the KO Lambert solver, $\mathbf{KO_{vnoJ}}$. Subsequently, the initial velocity found using the BMW Lambert solver for the single revolution case, $\mathbf{BMW_v}$, is propagated using the numerical propagator in a two-body system with J_2 effects. The norm of the difference between the final position that the satellite reaches and the desired final position is 7.81 km. Finally, the initial velocity found using the KO for the single revolution case where J_2 effects have been considered is propagated using the numerical propagator in a two-body system with J_2 effects. The norm of the difference between the final position that the satellite reaches and the desired final position is 0.00401 km. Therefore, when considering the unperturbed system for the single-revolution case, the BMW algorithm has increased accuracy compared to KO for finding the initial velocity that the satellite needs in order to attain the desired final position. However, the second velocity found using the KO, $\mathbf{KO_{vJ}}$, gets the satellite closer to the desired

Table 4.1: Difference Between Attained Final Position and Desired Final Position of Transfer

	BMW	KO
System w/o J_2	2.543 x10^{-11} km	0.00421 km
System w/ J_2	7.81 km	0.00401 km

final position when propagated in a two-body system with J_2 effects compared to using the velocity found using the BMW algorithm which does not take into account J_2 effects. These results are summarized in Table 4.1.

The second measure of accuracy of the solutions found using KO is demonstrated by a comparison with a numerical integration of the J_2 dynamical system using a Runge-Kutta scheme of order 4-5. This builds on the previous measure of accuracy by exploring the effects of changing the order of the basis functions used in the KO solution. Using the initial conditions from Section 4.2.1, the KO solutions for order 3 in the basis functions are compared to a numerical integration of the equations in Figure 4-3 for a time of flight of 3600 s. The error of the transfer orbit solution is in the order of magnitude of kilometers. The order of the KO basis functions is increased to order 7. This increase allows for the non-linearities of the J_2 dynamical system to be better captured in the solution. Figure 4-4 compares the solution found using the KO with the numerical integration for order 7 in the basis functions. The error in the solution has decreased to a maximum of about 70 cm, smaller than the error of the order 3 results by 4 orders of magnitude. Hence, increasing the order of the KO basis functions, decreases the error with respect to a numerical integration of the solution, demonstrating how an increase in the order leads to the solution approaching the real evolution of the system.

4.4 Various Initial Conditions

Optimal transfer orbits for various different initial and final position vectors and times of flight can be solved using the same procedure as described in Sections 4.2.1 and 4.2.2 as shown in Figure 4-5. These solutions are found using state transition matrices

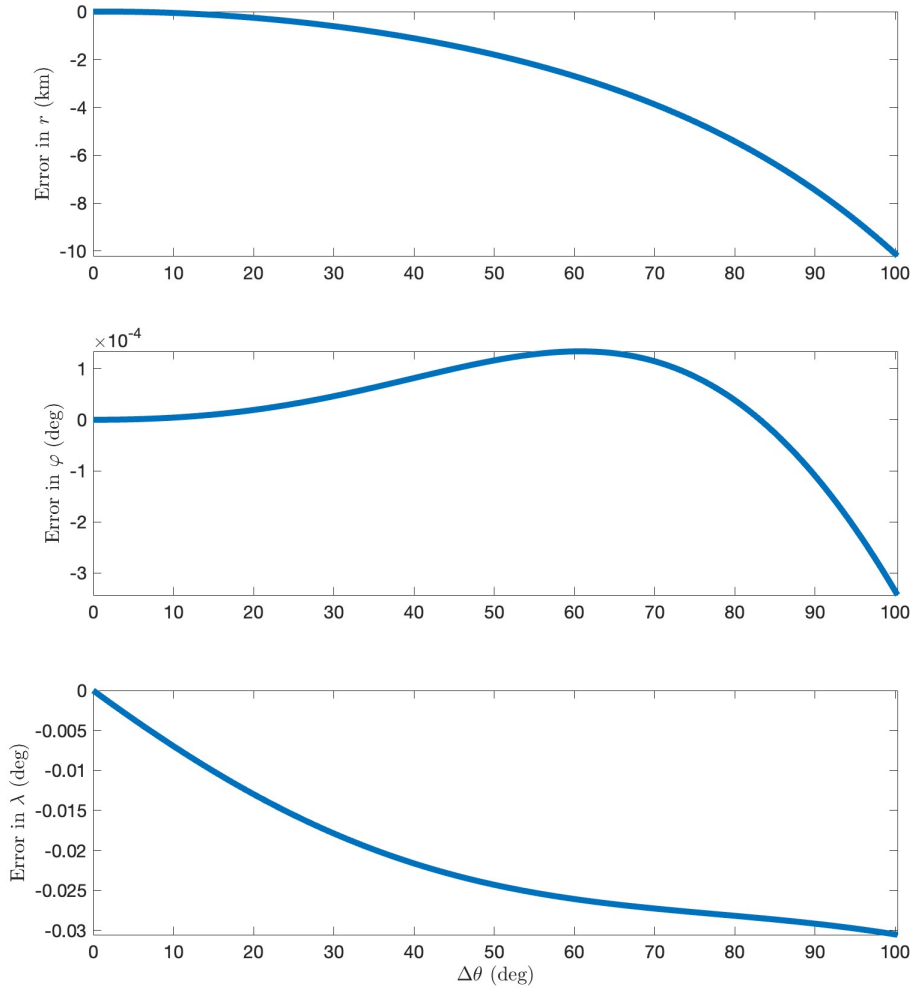

Figure 4-3: Performance Error of 3rd Order KO Solution

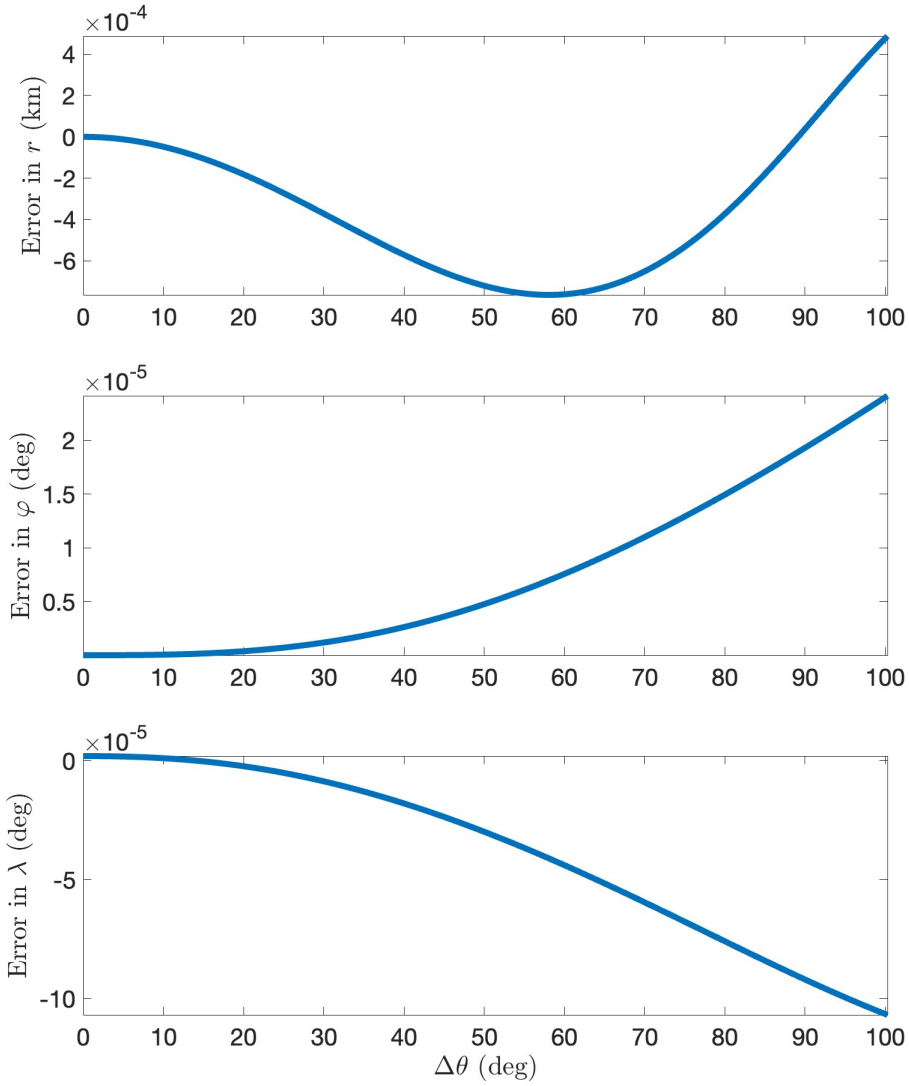

Figure 4-4: Performance Error of 7th Order KO Solution

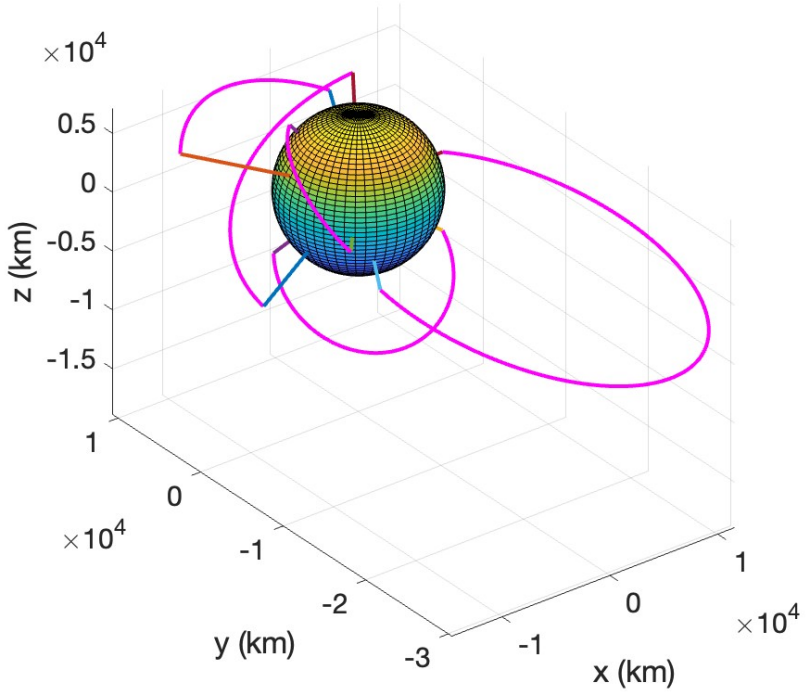

Figure 4-5: Single Revolution Optimal Trajectories with J_2 Effects for Different Initial Conditions

and without recalculating the KO matrix. This section demonstrates the versatility of using the KO to solve Lambert's problem by presenting solutions for transfer orbits to a highly eccentric orbit, to an orbit at the critical inclination, and to a circular geostationary orbit.

4.4.1 Transfer to a Highly Eccentric Orbit

Transfer orbits to highly eccentric orbits such as the Molniya orbit are desired for some communication satellites. Such orbits allow satellite operators to effectively view far northern latitudes that other orbits including geostationary equatorial orbits could not effectively allow for. An example of a Molniya orbit that a satellite could

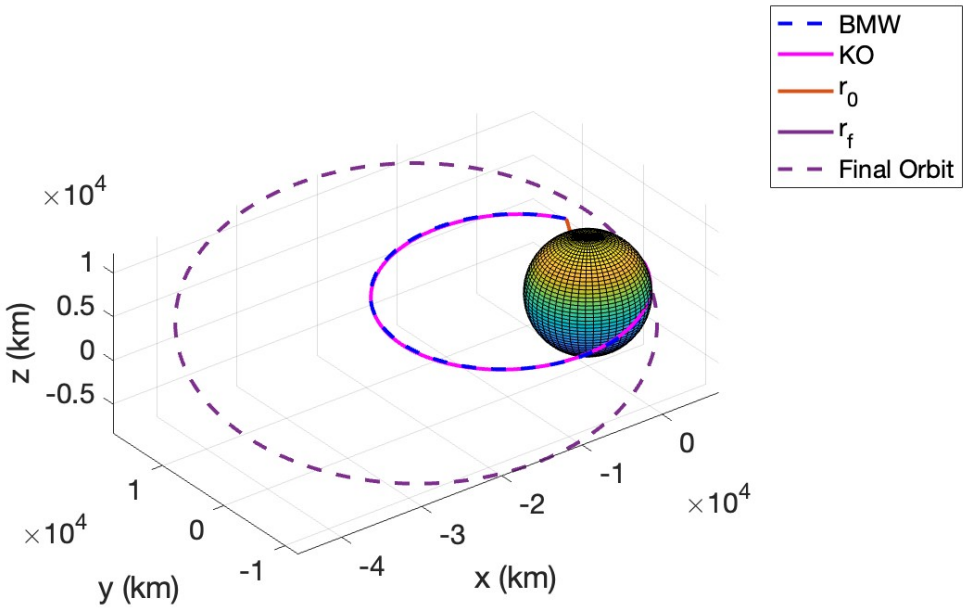

Figure 4-6: KO and BMW Transfer Orbits to a Highly Eccentric Orbit

transfer to, in familiar Keplerian coordinates, is:

$$\begin{aligned} a_f = 26,600 \text{ km}, \quad e_f = 0.74, \quad i_f = 80 \text{ deg}, \\ \omega_f = 270.0 \text{ deg}, \quad \Omega_f = 0.0 \text{ deg}, \quad \nu_f = 0.0 \text{ deg} \end{aligned} \tag{4.5}$$

Coordinate transformations from Keplerian to Cartesian, then from Cartesian to the orbital elements in Section 3.5 are performed to solve for the optimal transfer orbits. An optimal transfer orbit from the same initial vector as in Section 4.2.1 and a time of flight of 5,000 seconds is solved using the KO method with order 7 basis functions. The transfer orbit is shown in Figure 4-6 solved by using the KO theory as well as solved by using the algorithm by Bate, Mueller, and White. The error between the KO solution propagated over time and that of the solution propagated using a numerical integration method is plotted in Figure 4-7. The error in r is on the order of 10^{-1}km but is decreasing as $\Delta\theta$ increases.

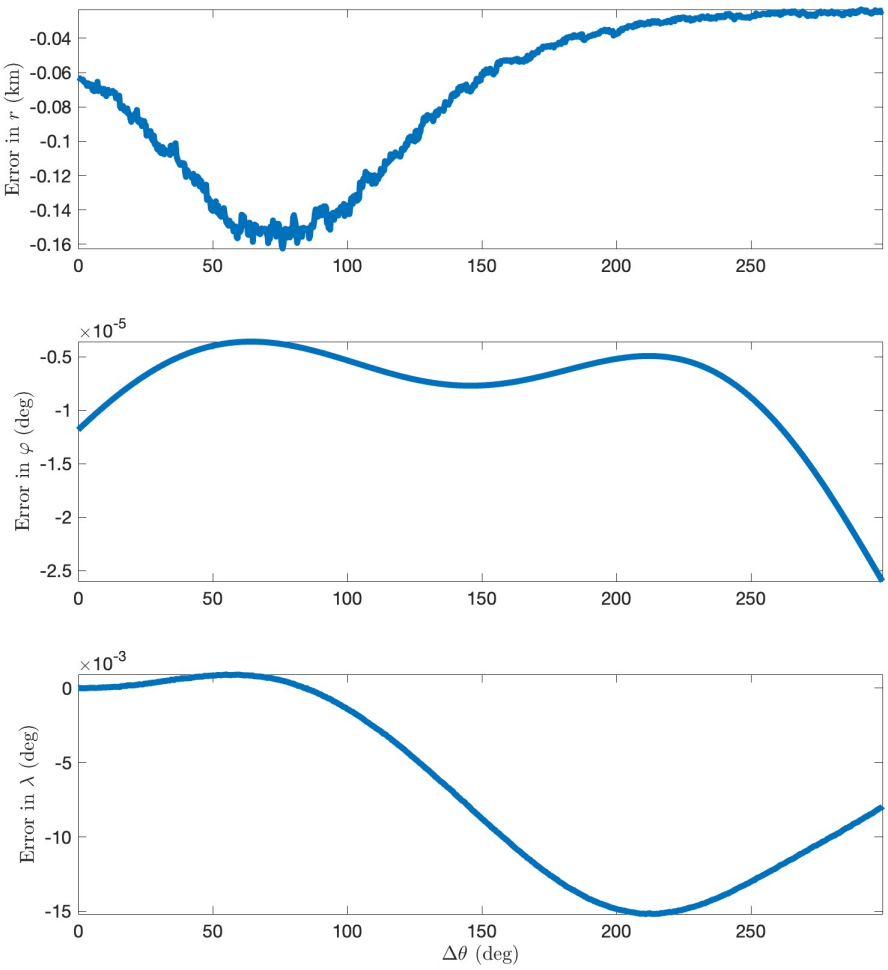

Figure 4-7: Error of KO Transfer Orbit to a Highly Eccentric Orbit

4.4.2 Transfer to an Orbit at the Critical Inclination

Specific Lambert solvers, as documented in existing literature, might encounter functionality issues in proximity to the critical inclination, potentially resulting in the derivation of imaginary solutions. These imaginary solutions stem from the fact that Lambert's problem is not well-posed for some configurations such as solving for optimal transfer orbits near the critical inclination. One such solver is the Gauss-Legendre algorithm that has difficulties solving for optimal transfer orbits near the critical inclination. Hence, it is of interest to show that solutions to Lambert's problem for transfer orbits near the critical inclination can be solved using the KO method. Let the final orbit be located at the critical inclination:

$$\begin{aligned} a_f = 15,029 \text{ km}, \quad e_f = 0.433, \quad i_f = 63.4 \text{ deg}, \\ \omega_f = 30.19 \text{ deg}, \quad \Omega_f = 30.21 \text{ deg}, \quad \nu_f = 0 \text{ deg} \end{aligned} \tag{4.6}$$

Using order 7 basis functions in the KO method, the transfer computed for a time of flight of 7000 s is shown in Figure 4-8 along with the transfer computed using the BMW algorithm. The error between the KO transfer to the critical inclination and the numerical propagation of the solution is shown in Figure 4-9. The error in r is on the order of a couple of meters.

4.4.3 Transfer to a Geostationary Equatorial Orbit

A circular geostationary equatorial orbit (GEO) is an orbit where a satellite always remains above the same point on the Earth's equator. The angular velocity of the radial connecting the satellite and Earth's center must match the angular velocity of the Earth itself, being 2π radians per sidereal day. Global weather satellites and communications satellites are placed in GEO orbits due to the large portion of the Earth's surface visible from the high altitude. Furthermore, satellites in GEO appear motionless in the sky which reduce the need for tracking them using ground stations [24]. Furthermore, most rockets launch satellites to LEO, after which these satellites must complete transfers in order to reach GEO. Hence, solving Lambert's problem

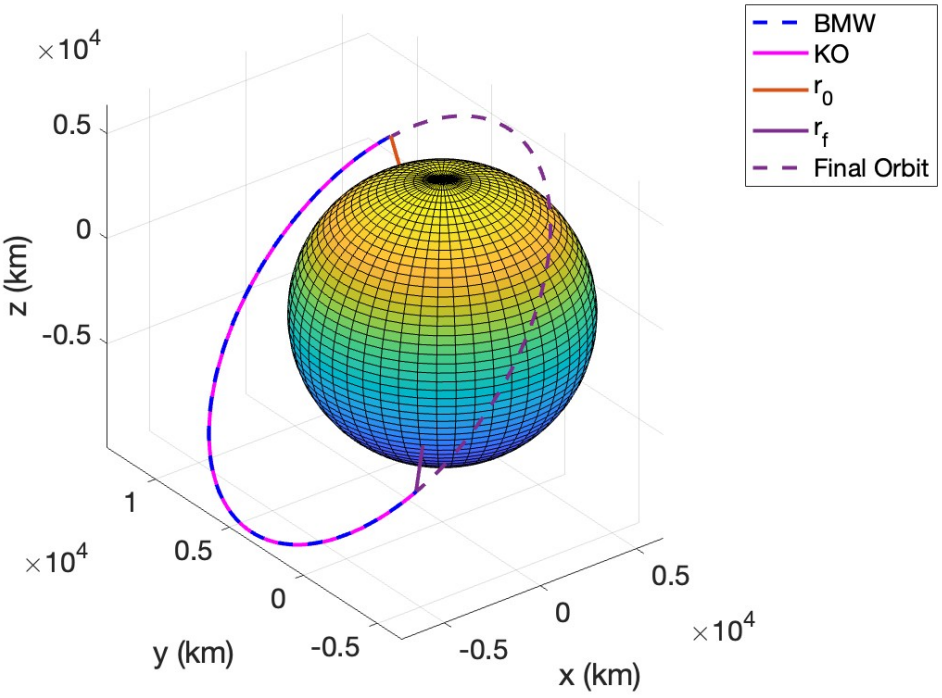

Figure 4-8: KO and BMW Transfer Orbits to the Critical Inclination

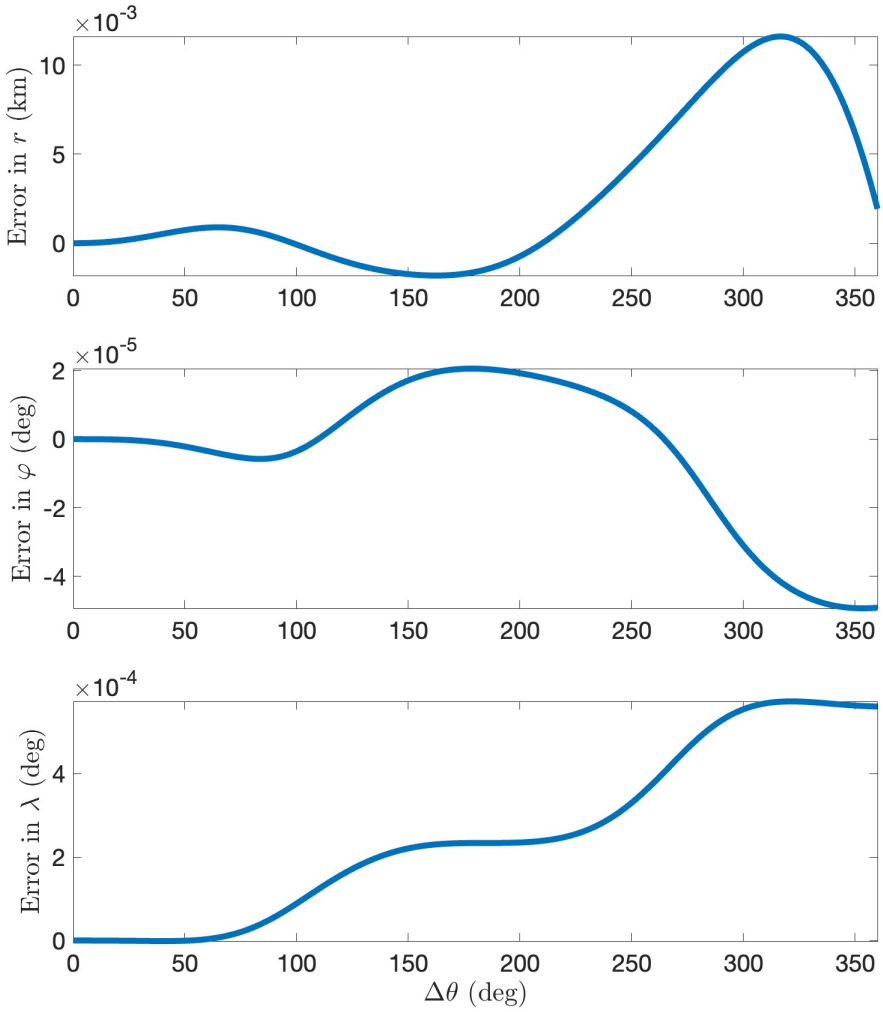

Figure 4-9: Error of KO Transfer Orbit to the Critical Inclination

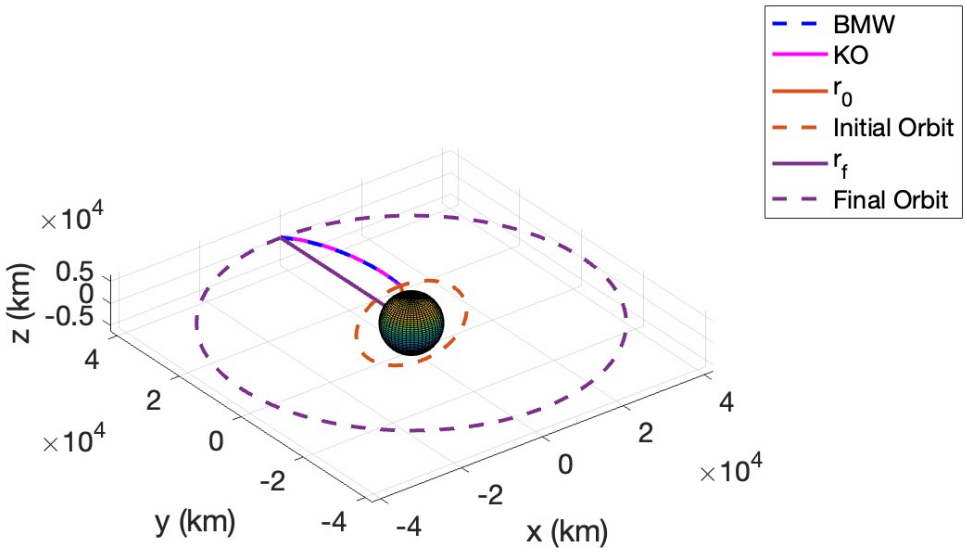

Figure 4-10: KO and BMW Transfer Orbits to GEO

for these transfer orbits presents an interesting use case. The initial conditions of a transfer to a GEO orbit are,

$$\begin{aligned} \mathbf{r}_0 &= [5000, \quad 10,000, \quad 2100] \text{ km} \\ \mathbf{r}_f &= [0, \quad 42,164, \quad 0] \text{ km} \end{aligned} \tag{4.7}$$

with a time of flight selected as 10,000 s. The transfer orbit computed using the KO method with order 7 basis functions is shown in Figure 4-10. The initial circular orbit and the GEO final orbit are plotted as well. The error between the KO transfer to GEO and the numerical propagation of the solution is plotted in Figure 4-11. The error can be seen to be on the order of a couple of km at the beginning of the propagation but quickly increases to order 10^1 km and approaches 10^2 km near the end of the propagation.

The smallest error between KO and the numerical propagation of the solution

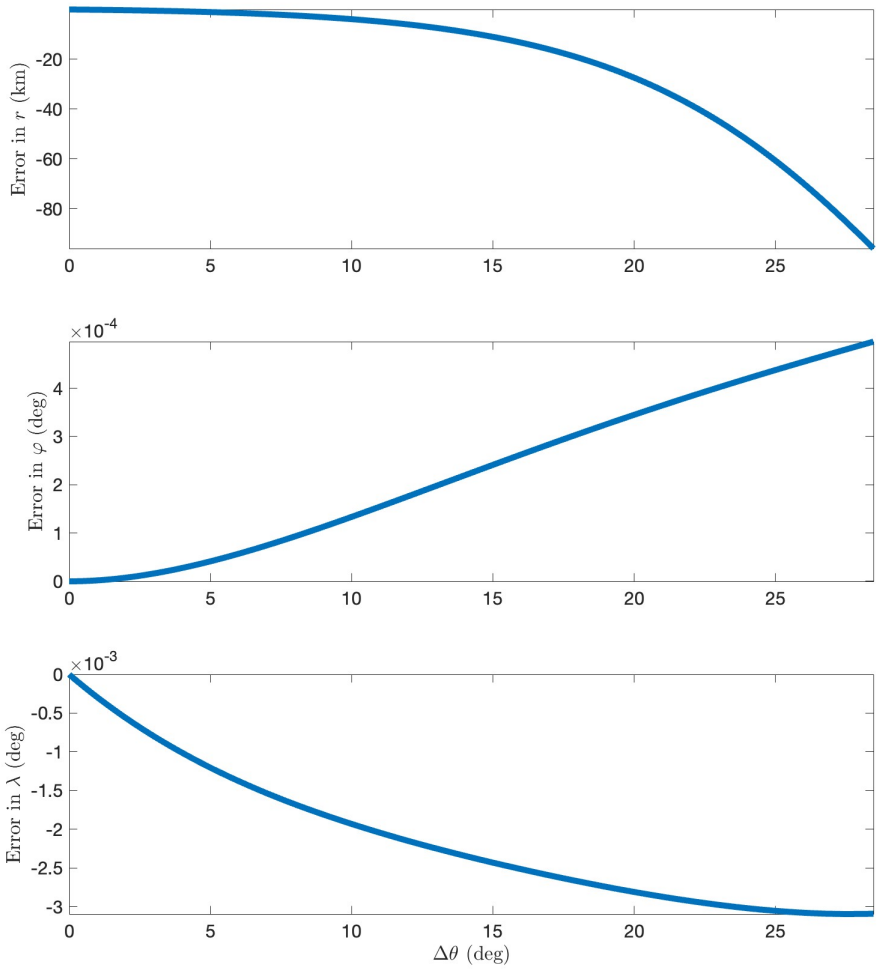

Figure 4-11: Error of KO Transfer Orbit to GEO

occurs in the case of the transfer to an orbit at the critical inclination where the error in r is on the order of a couple of meters. The largest error between KO and the numerical propagation of the solution occurs in the case of the transfer to GEO where the error is on the order of 10^1 km.

4.5 Minimum Energy and Minimum ΔV Solutions

Solving specific cases of Lambert's problem concerns the use of a cost function to find an optimal orbit trajectory. In this section, cost functions corresponding to the minimum energy transfer orbit and the minimum Δv transfer orbit are explored. The minimum energy and minimum Δv solutions to Lambert's problem are crucial to modern space missions that have various fuel and time constraints. Both the minimum energy and minimum Δv solutions are found in this section using the KO while taking into account J_2 effects.

4.5.1 Minimum Energy Solution

First, the specific energy is selected as the cost function to solve Lambert's problem. The specific energy, E, is given by

$$E = -\frac{\mu}{2a} \tag{4.8}$$

where a is the semi-major axis and is calculated for each transfer orbit from the initial Cartesian coordinates using

$$a = \frac{1}{\frac{2}{|\mathbf{r}_0|} - \frac{|\mathbf{v}_0|^2}{\mu}}. \tag{4.9}$$

Negative specific energy solutions indicate elliptical transfer orbits, while positive specific energy solutions indicate hyperbolic transfer orbits. Specific energy of 0 kJ/kg corresponds to a parabolic transfer orbit. This Thesis concerns solutions that transfer satellites from one point to another and hence focuses on only elliptical transfer orbits. The minimal specific energy transfer orbit is found by calculating

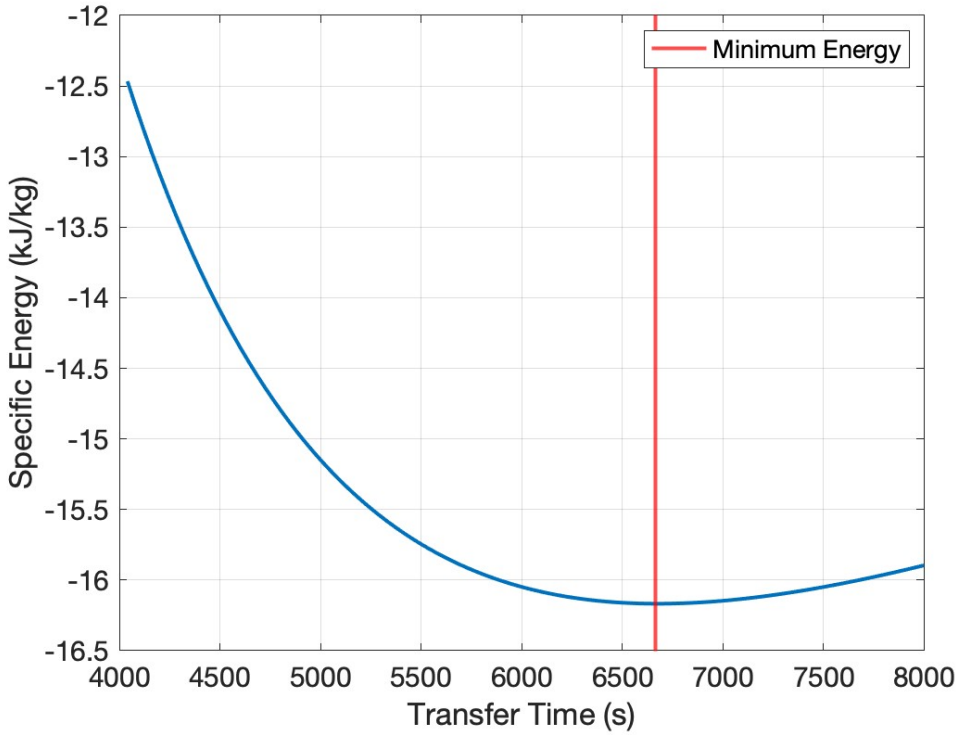

Figure 4-12: Specific Energy of Each Transfer Orbit

the specific energy of each possible transfer orbit for different times of flight. For the initial conditions considered in Section 4.2.1, in Equation 4.1, the minimum specific energy transfer orbit is found to have a time of flight of 6630 s which corresponds to a semi-major axis of $12,328$ km and a minimum specific energy of -16.2 kJ/kg. The specific energies for transfer times near the time corresponding to the minimum specific energy solution are plotted in Figure 4-12. The minimum specific energy transfer orbit is plotted in Figure 4-13.

4.5.2 Minimum ΔV Solution

The Δv is selected as another cost function to solve Lambert's problem. The minimum Δv Lambert's problem concerns finding the optimal transfer orbit between an initial position vector on an orbit and a final position vector on another orbit that minimizes the change in velocity required for the transfer [11]. The total Δv of the transfer orbit

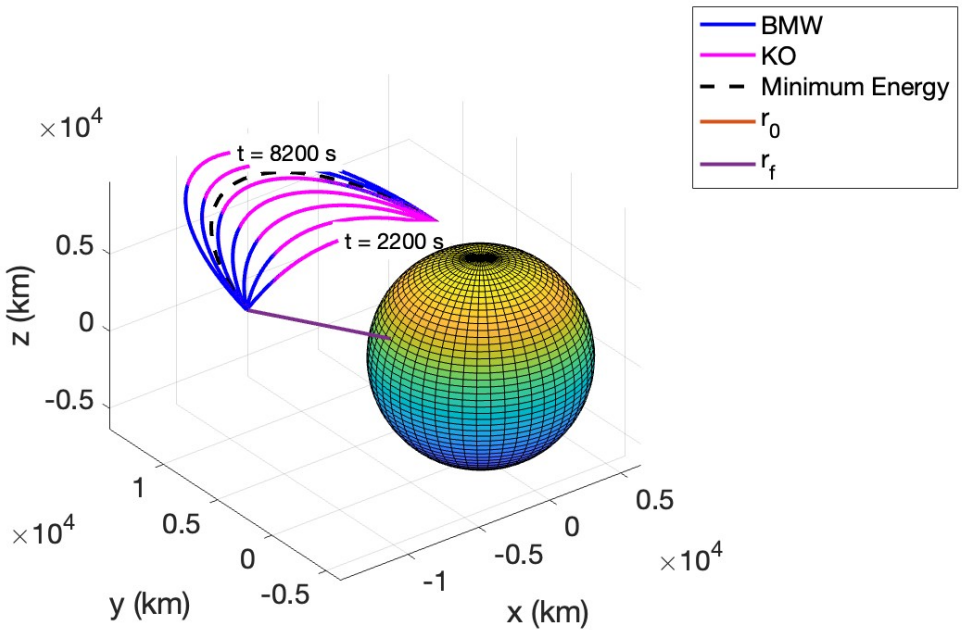

Figure 4-13: Minimum Energy Single Revolution Solution with J_2 Effects

is given by,

$$\Delta v_{\text{total}} = \Delta v_1 + \Delta v_2 \tag{4.10}$$

where Δv_1 is the change in the velocity from the initial orbit to the transfer orbit and Δv_2 is the change in the velocity from the transfer orbit to the final orbit,

$$\Delta v_1 = \sqrt{(v_{x_2} - v_{x_1})^2 + (v_{y_2} - v_{y_1})^2 + (v_{z_2} - v_{z_1})^2}$$
$$\Delta v_2 = \sqrt{(v_{x_3} - v_{x_2})^2 + (v_{y_3} - v_{y_2})^2 + (v_{z_3} - v_{z_2})^2}.$$

Uniform circular motion orbits are assumed for the initial orbit the satellite is transferring from and for the final orbit the satellite is transferring to. The Δv of each possible transfer orbit for different times of flight are found and then the minimum is taken. For the initial conditions considered in Equation 4.1, the minimum Δv transfer orbit is found to correspond to a time of flight of 4598 s with a Δv of 1.90 km/s. The Δv's for transfer times near the time corresponding to the minimum Δv solution are plotted in Figure 4-14. The minimum Δv transfer orbit is plotted in Figure 4-15 along with the initial and final circular orbits and the minimum energy transfer orbit for reference.

4.5.3 Pork-Chop Plots and ΔV: Mapping Efficient Trajectories

Using the method described in Section 4.5.2, it is possible to calculate the minimum Δv trajectory given any initial and final position vectors on two generic elliptic orbits. Hence, it is possible to produce "pork-chop" plots that identify the best departure and arrival orbital positions on these orbits [7] [56]. Two generic elliptic orbits are chosen and the true anomaly of each is divided into increments of 20°. The minimum Δv direct transfer orbit connecting each possible initial true anomaly and each possible final true anomaly along the elliptic orbits is calculated. Values are interpolated so that the minimum Δv is calculated every 1° in true anomaly. The resulting matrix is displayed as a contour map in Figure 4-16. A generic pattern can be seen in Figure 4-

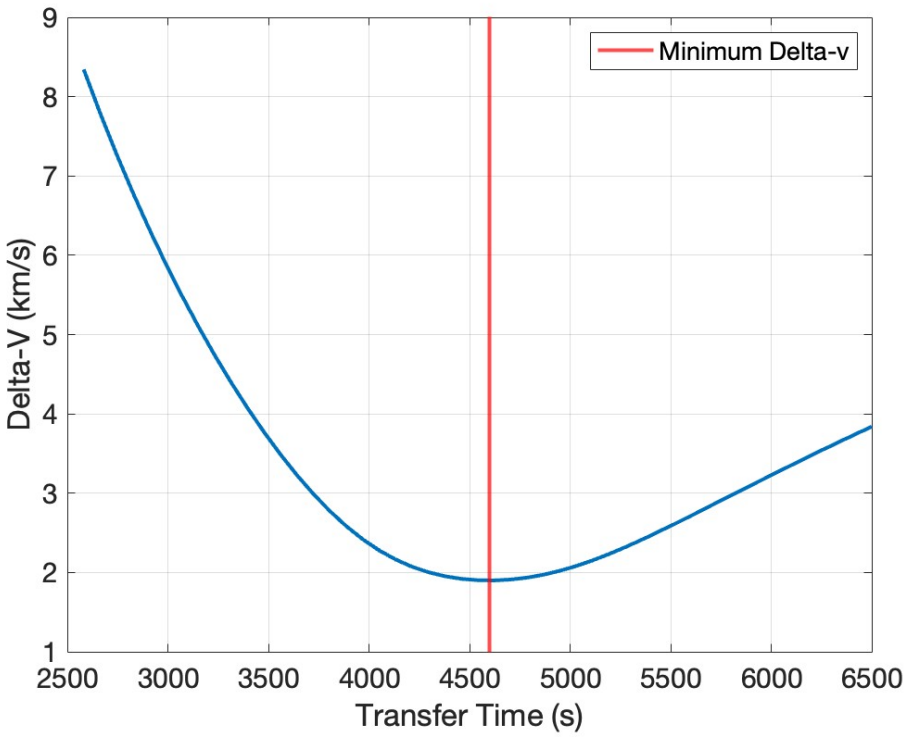

Figure 4-14: Minimum ΔV of Each Transfer Orbit

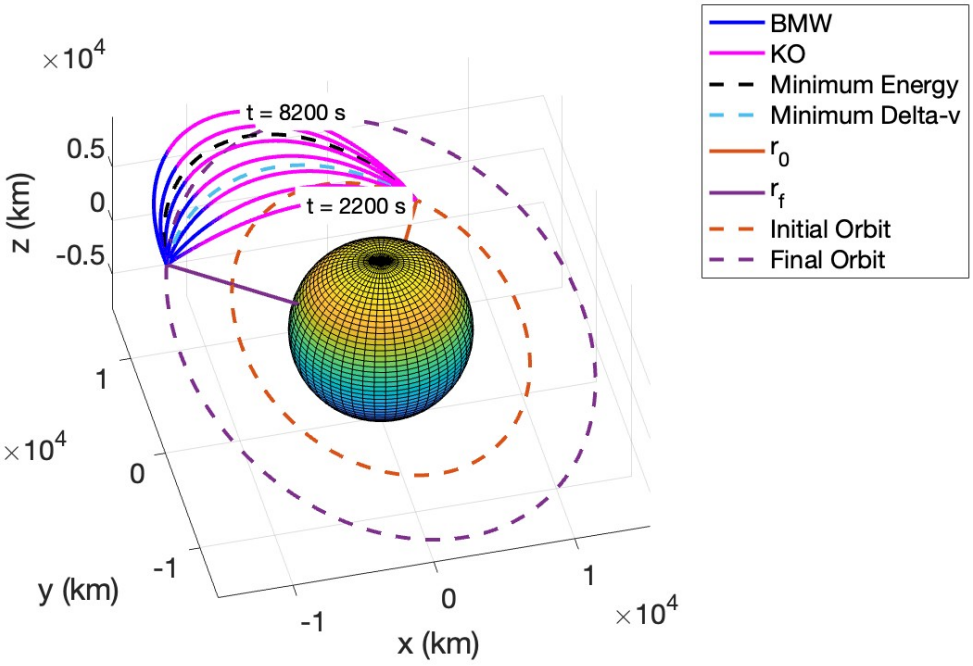

Figure 4-15: Minimum Energy and Minimum ΔV Single Revolution Solution with J_2 Effects

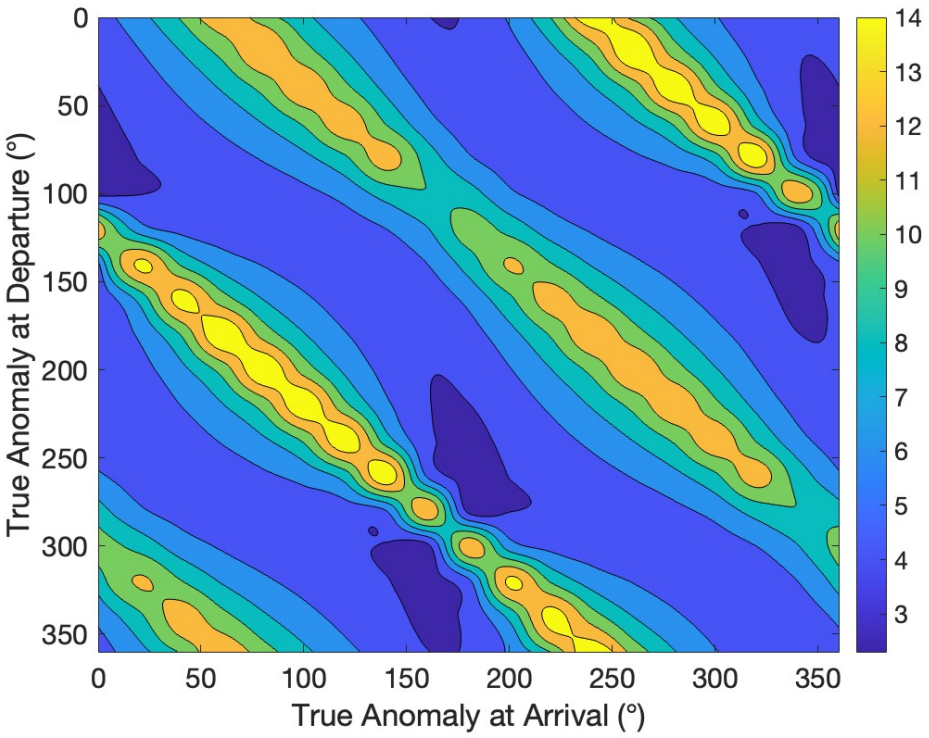

Figure 4-16: Contour Map of the Minimum ΔV Direct Transfer Between Two Generic Elliptical Orbits

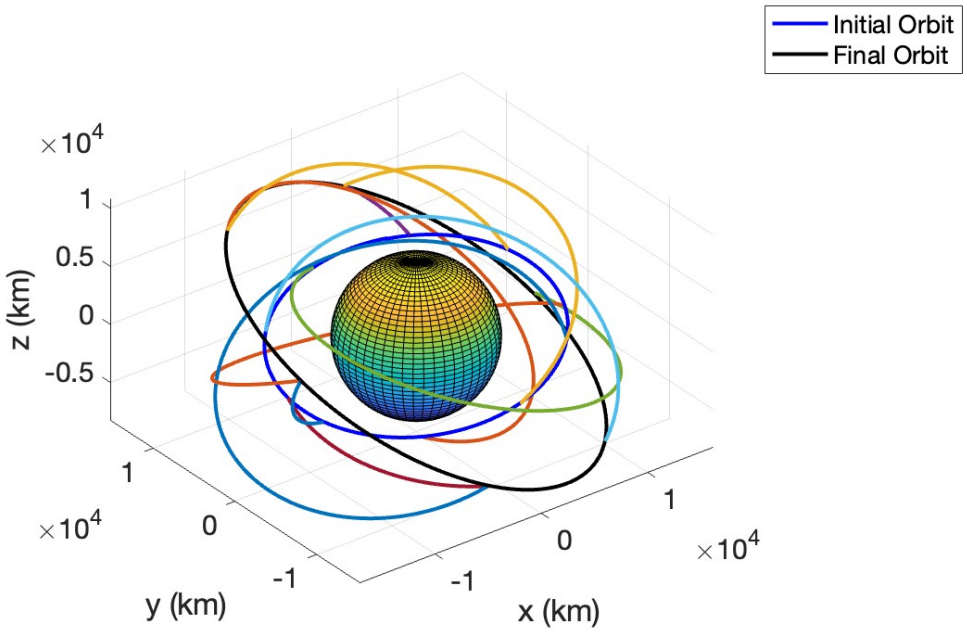

Figure 4-17: Sample of Minimum ΔV Direct Transfer Orbits Between Two Generic Elliptical Orbits

16 where diagonals across the matrix have similar Δv values. The difference between the true anomaly at arrival and the true anomaly at departure is constant along these lines. The Δv required to transfer between these true anomalies is a significant factor in determining the overall Δv requirements for the trajectory. The constant true anomaly difference along each diagonal results in similar minimum Δv values for each trajectory on that diagonal.

A sample of 10 of the minimum Δv transfer orbits from Figure 4-16 are displayed in Figure 4-17 along with the chosen initial and final generic elliptical orbits. It is important to note that the initial and final generic elliptical orbits, as well as, the transfer orbits are all chosen to be prograde. Given that the initial and final generic elliptical orbits are chosen to be prograde, prograde transfers are generally more efficient than retrograde transfers between these chosen orbits.

A 3-D "pork-chop" plot of the matrix plot from Figure 4-16 is shown in Figure

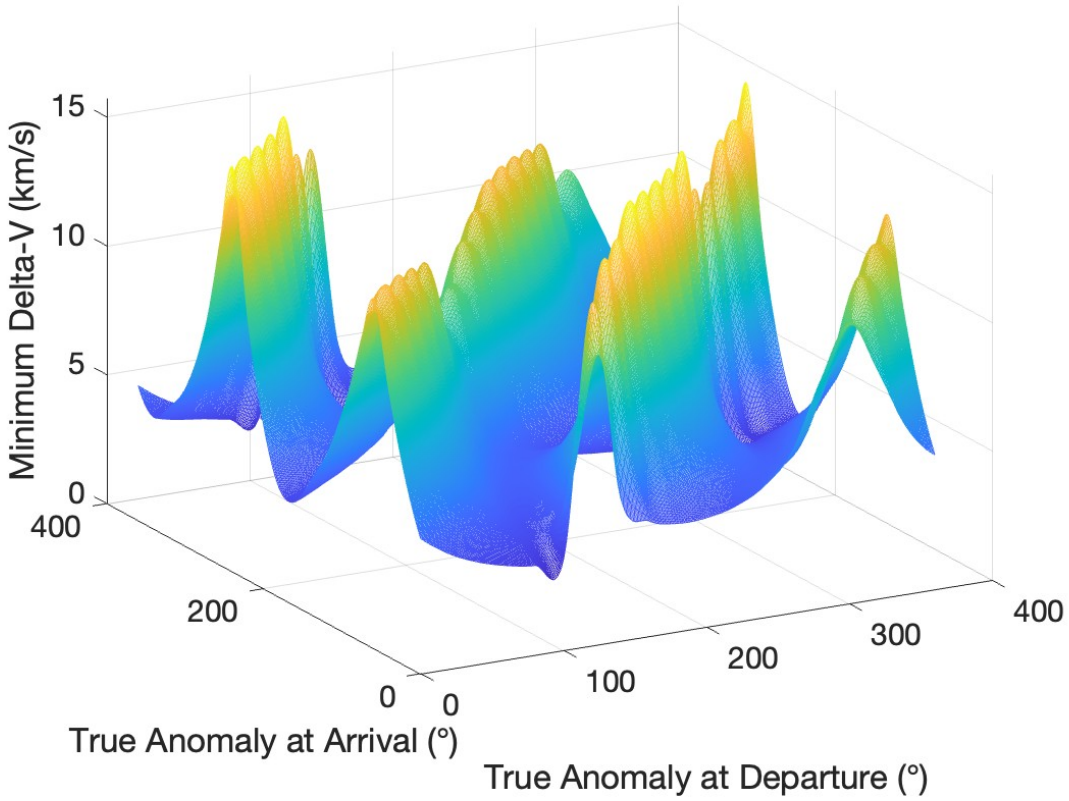

Figure 4-18: "Pork-Chop" of the Minimum ΔV Direct Transfer Orbits Between Two Generic Elliptical Orbits

4-18. The 3-D pork-chop plot and the contour plot can be used to identify the best departure and arrival orbital positions that correspond to the overall minimum Δv transfer. This overall minimum occurs at a value of 140 ° in true anomaly at departure and 340 ° in true anomaly at arrival with a minimum Δv of 3.46 km/s. Finally, Figure 4-19 shows the three-dimensional geometry of the optimal orbit transfer trajectory along with the initial and final orbits.

As a comparison, a Runge-Kutta scheme of order 4-5 is used to solve for the velocities of each orbit transfer in the perturbed system for each possible time of flight using the BMW algorithm as the initial guess. This method completes a numerical integration of Equation 3.10 in Cartesian coordinates when solving for the velocities using the Levenberg-Marquadt algorithm. The orbit transfer with the minimum Δv is calculated for each combination of increments in true anomaly on the two generic

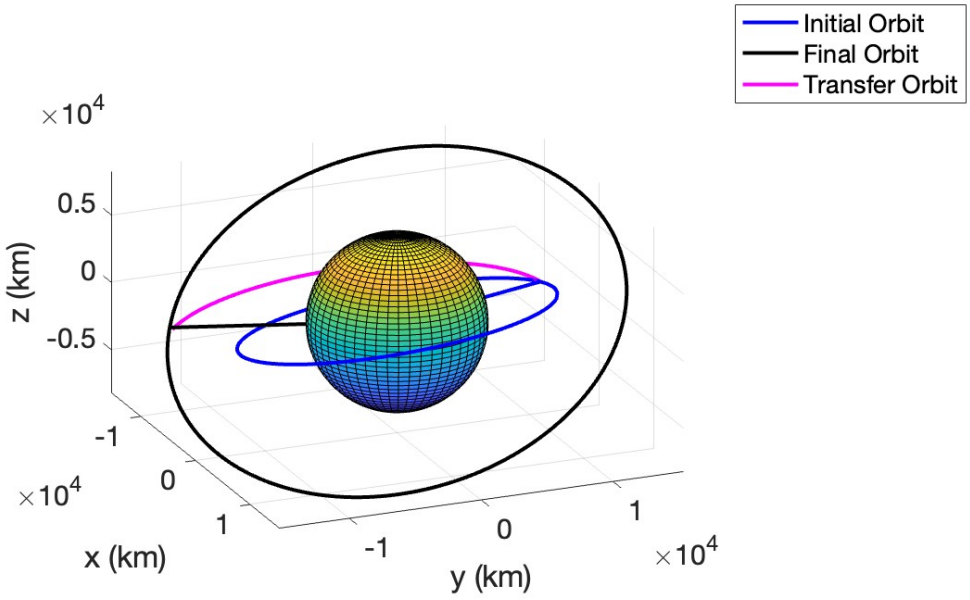

Figure 4-19: Optimal Transfer Orbit for the Pork-Chop Minimum ΔV

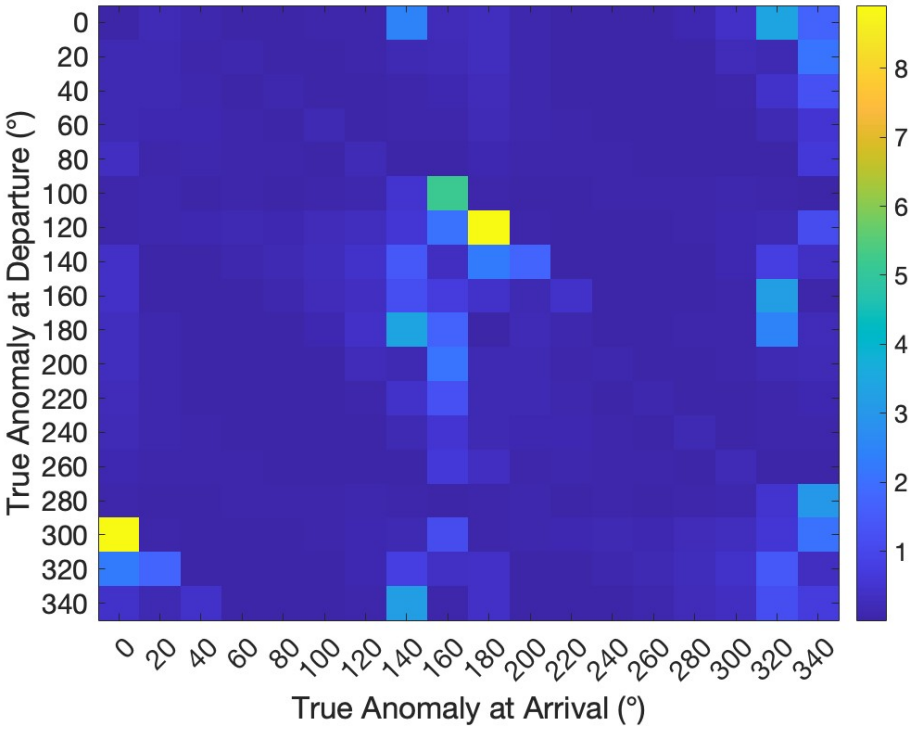

Figure 4-20: Relative Error of the Minimum ΔV Solutions

elliptical orbits. A similar contour map to the one in Figure 4-16 is created using this numerical integration method. The relative error between the KO minimum Δv matrix, M_{KO}, and the numerical integration minimum Δv matrix, $M_{numerical}$ is computed using,

$$\text{Error} = \frac{|M_{numerical} - M_{KO}|}{M_{numerical}} \tag{4.11}$$

The relative error is displayed in Figure 4-20 as a contour map where the color bar depicts the relative error as a percent. The mean relative error is 0.339% with the minimum value being $6.21 * 10^{-6}$ % and the maximum value being 8.91%. Hence, on average solving the Minimum Δv Lambert's problem using the KO leads to accurate solutions that are within 0.339% of a numerical method's solutions.

4.6 Lambert's Problem Multiple Revolutions

The solution to the multiple revolution Lambert's problem is now presented. These solutions involve finding optimal transfer orbits that complete one, or more, revolutions around the gravitational body between the initial and final position vectors.

4.6.1 Unperturbed System

The multiple revolution solution is first solved in the unperturbed dynamical system. The initial and final position vectors from Section 4.2.1 are taken as the initial conditions. The period of a full orbit for the trajectory found in Section 4.2.1 is calculated to be $T = 28,175$ s. A large transfer time corresponding to three orbital periods of $84,463$ s is chosen in order to solve for multiple revolutions. These multiple revolutions solutions are found by adding $2\pi N$ to $\Delta\theta$ in Equation 4.2, where N represents the number of revolutions. The new value for $\Delta\theta$ is directly incorporated into the KO solution, resulting in a new polynomial map. This polynomial map connects the initial state to the final state taking into account the specified number of revolutions. Hence, a KO polynomial map is created for each number of revolutions without the need to recalculate the KO matrix, a benefit from using the KO theory. This entails benefits because the zonal representation uses true anomaly as its independent variable. The 0, 1, 2, and 3 complete revolution solutions to Lambert's problem with a time constraint of $84,463$ s are plotted in Figure 4-21.

4.6.2 Perturbed System

The perturbed dynamical system is considered and the optimal trajectories to the multiple revolutions Lambert's problem are solved for. The position vectors from Equation 4.1 are considered. The possible solutions to the multiple revolutions Lambert's problem are shown in Figure 4-22 for a variety of transfer times and semi-major axes. This figure presents the comprehensive solution space, encapsulating both direct transfer orbits and transfer orbits that complete multiple revolutions. It offers an entire view of the potential transfers a satellite can take between the specified po-

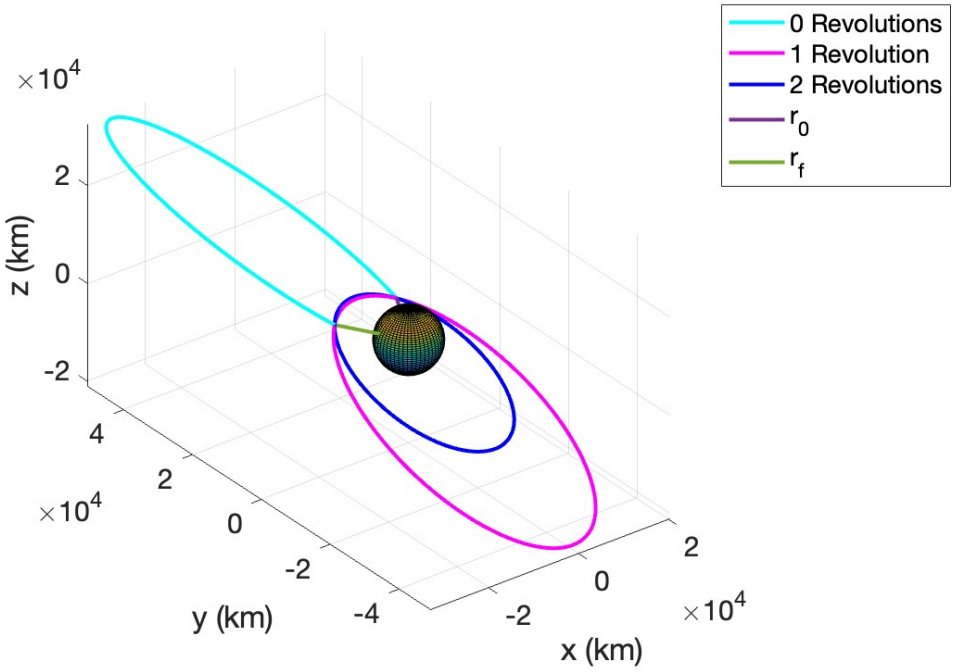

Figure 4-21: Multiple Revolutions Orbit Trajectories without J_2 Effects

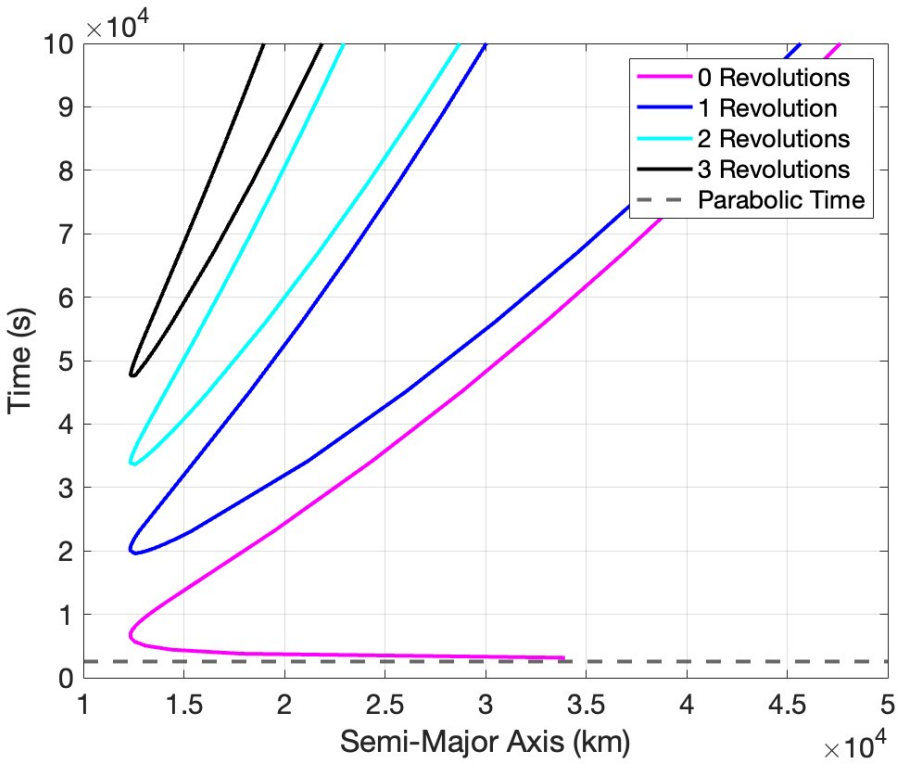

Figure 4-22: Semi-Major Axes and Potential Timeframes for Multiple Revolution Solutions to Lambert's Problem

sition vectors. There are seven possible orbital trajectories for transfer times greater than about 4800 s: two possible multiple revolutions transfer orbits for $N = 1, 2$ and 3 and one possible solution for a single revolution orbit transfer. Such times are too long for another single revolution orbit transfer solution as this other possible solution approaches the time corresponding to a parabolic transfer orbit for increasing semi-major axis.

The 0, 1, 2, and 3 revolutions solutions transfer orbits are plotted in Figure 4-23. These correspond in color to the multiple revolutions solutions plotted in Figure 4-22. Some of these multiple revolution solutions are not feasible due to having small semi-major axes that cause their orbital trajectories to pass through the Earth for the time constraint considered.

The specific energies, Δv, and semi-major axes for the 0, 1, 2, and 3 complete revolution orbit transfers are shown in Table 4.2 The specific energy decreases as

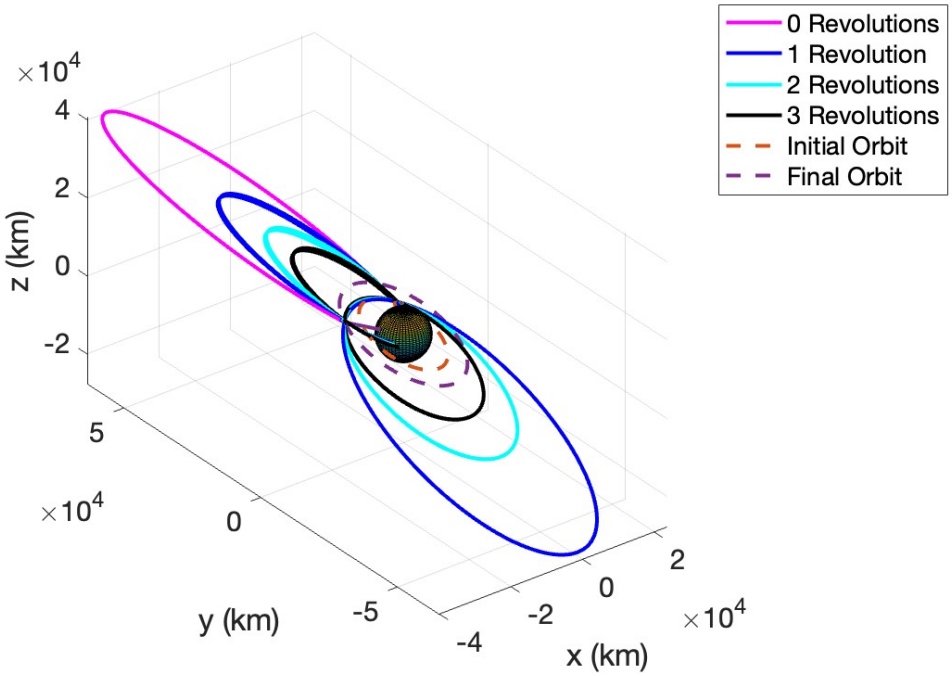

Figure 4-23: Multiple Revolutions Orbit Trajectories with J_2 Effects

Table 4.2: Specific Energies, ΔV, and Semi-Major Axes for Multi-Revolution Transfer Orbits

Number of Revolutions	Semi-Major Axis	Specific Energy	ΔV
Initial orbit	11,376 km		
Final orbit	16,383 km		
0	42,740 km	-4.66 kJ/kg	12.85 km/s
1	40,634 km	-4.90 kJ/kg	5.45 km/s
1	26,969 km	-7.39 kJ/kg	11.62 km/s
2	25,532 km	-7.81 kJ/kg	4.30 km/s
2	20,622 km	-9.66 kJ/kg	10.47 km/s
3	19,433 km	-10.26 kJ/kg	3.24 km/s
3	17,064 km	-11.68 kJ/kg	9.30 km/s

the number of revolutions of the transfer orbit increase for the specified transfer time. Furthermore, as the number of revolutions of the orbit transfer increases, the required Δv decreases. The biggest difference in Δv is between the direct transfer orbit and that of a transfer orbit that takes 3 revolutions.

4.7 Error Correction

Considering the initial conditions and problem formulation in Section 4.2, this section explores an error correction method that can be used to decrease the difference between the final position targeted at and the final position attained. The velocity needed to reach the final position is recalculated during the transfer, hence increasing the accuracy of the transfer. The corresponding required Δv is also found. As an example, the velocity is recalculated twice during the transfer in Figure 4-24: once at 1/3 of the transfer and a second time at 2/3 of the transfer. The norm of the difference between the final position that the satellite reaches and the desired final position is calculated at the end of each of these 2 parts of the transfer. The norm decreases from 7.56 km to 2.80 km and finally to 0.88 km at the final calculation of the velocity. Hence, showing how a decrease in error can be attained by recalculating the solution during the transfer. The Δv at these two steps required for such a decrease in error are 0.0015 km/s and 0.0046 km/s respectively.

4.8 Multi-Impulse Lambert Solution

The multi-impulse solution to Lambert's problem is now presented. Once again, the initial and final position vectors from Equation 4.1 in Section 4.2.1 are taken as the initial conditions. A circular prograde initial orbit for the spacecraft is assumed with velocity,

$$\mathbf{v}_0 = [-5.203,\ \ 2.7419,\ \ -0.6673] \text{ km/s} \tag{4.12}$$

A two-impulse solution is considered. An intermediary position, $\mathbf{r}_{imp}$ is sought for where a second impulse would take place. Hence, one impulse would occur at $\mathbf{r}_0$

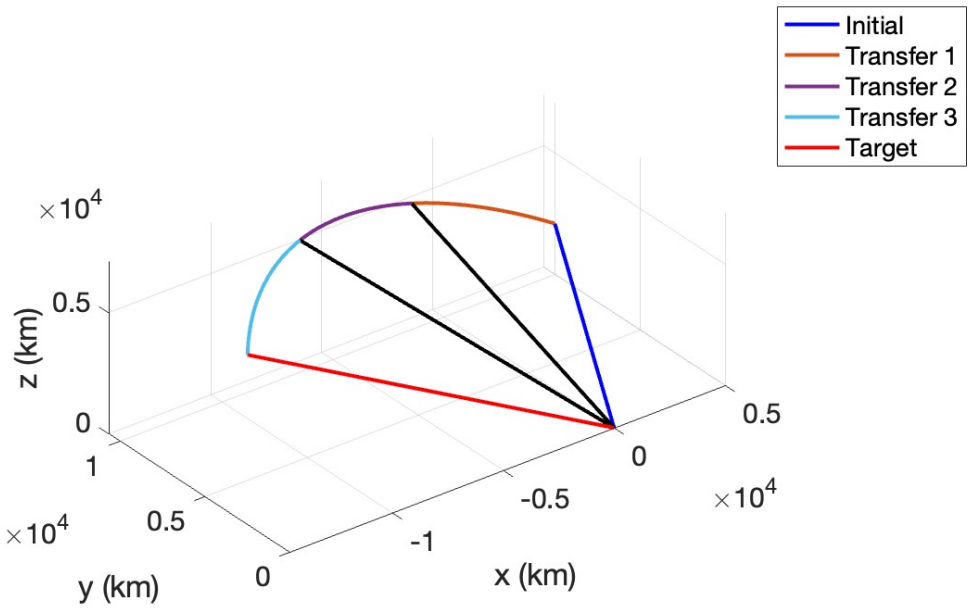

Figure 4-24: Error Correction Using Three Transfers

for the change in velocity from the initial circular orbit, $\mathbf{v}_0$, to the velocity required for the optimal first transfer orbit to $\mathbf{r}_{imp}$, denoted by $\mathbf{v}_1$. Then a second impulse would occur at $\mathbf{r}_{imp}$ for the change in velocity from the velocity at the end of the first transfer orbit, denoted by $\mathbf{v}_2$, to the velocity required for the optimal second transfer orbit to $\mathbf{r}_f$, denoted by $\mathbf{v}_3$. Hence, the objective is to minimize the total Δv of the multi-impulse transfer given by,

$$\Delta v_{\text{total}} = \Delta v_1 + \Delta v_2 \tag{4.13}$$

where

$$\Delta v_1 = \sqrt{(v_{x_1} - v_{x_0})^2 + (v_{y_1} - v_{y_0})^2 + (v_{z_1} - v_{z_0})^2}$$
$$\Delta v_2 = \sqrt{(v_{x_3} - v_{x_2})^2 + (v_{y_3} - v_{y_2})^2 + (v_{z_3} - v_{z_2})^2}.$$

The position of $\mathbf{r}_{imp}$ in 3-D space is the point at which a second impulse maneuver would occur with the goal of minimizing the overall fuel consumption from the two impulses while connecting the initial and final position vectors. The transfers are constrained to be prograde. While considering retrograde orbit transfers would increase the solution space, the overall fuel consumption would likely be greater than using prograde transfer orbits since the initial orbit is prograde. Furthermore, if an assumption is made that the final orbit is prograde without adding a velocity constraint at $\mathbf{r}_f$, then the fuel consumption would be even more likely to be greater if one or both of the transfers were retrograde. A time-constrained solution and a time-open solution are presented.

4.8.1 Time-Constrained Solution

A time constrained solution is derived using two determined time durations. The first time duration is defined as the time a transfer to the position of the impulse would take assuming the initial circular velocity in Equation 4.12 was used. The second time duration is defined as the time a transfer to $\mathbf{r}_f$ would take assuming the velocity of the

first transfer was used. These time durations establish reasonable time constraints, enabling the derivation of a classical Lambert solution. A Genetic Algorithm is used to find the optimal position of $\mathbf{r}_{imp}$. It is a method inspired by the process of natural selection used to solve constrained and unconstrained optimization problems. The Genetic Algorithm generates a population of points at each iteration of searching for the optimal solution. On each iteration the best point in the population is selected as the one that has approached the most optimal solution. The next population for the next iteration is selected by computation using random number generators. Using such an algorithm allows for the space of possible solutions to be searched for efficiently. The algorithm avoids searching only one area of the search space and keeps exploring other areas that potentially contain better solutions. A population size of 10 was selected with 10 generations. The algorithm was run 10 times and the most optimal solution out of the ten runs was chosen. These parameters increase the likelihood of finding a globally optimal solution, as they mitigate the risk of settling on a sub-optimal solution due to the stochastic nature of the algorithm. The optimal position and resulting transfers are shown in Figure 4-25. The total Δv of this transfer is 4.4051 km/s. The time constraint for the first transfer was found to be 7,118 s and for the second transfer the time constraint was 10,198 s.

4.8.2 Time-Open Solution

Since the KO solution to Lambert's problem uses true anomaly as its independent variable, as evidenced in Equation 3.13, transfer orbits using true anomaly rather than time as the constraint can be found. Once the optimal position of the impulse is found, Equation 3.14 can be used to find the corresponding times of flight. Using the same parameters for the Genetic Algorithm as in Section 4.8.1, the optimal position and resulting transfers for the time-open solution are shown in Figure 4-26. The total Δv of this transfer is 3.5827 km/s. The corresponding time of flight for the first transfer is 14,541 s and for the second transfer the time of flight is 12,396 s. Furthermore, a direct transfer between the same initial and final position vectors with no time constraint results in a greater Δv of 3.8422 km/s. Such a transfer would

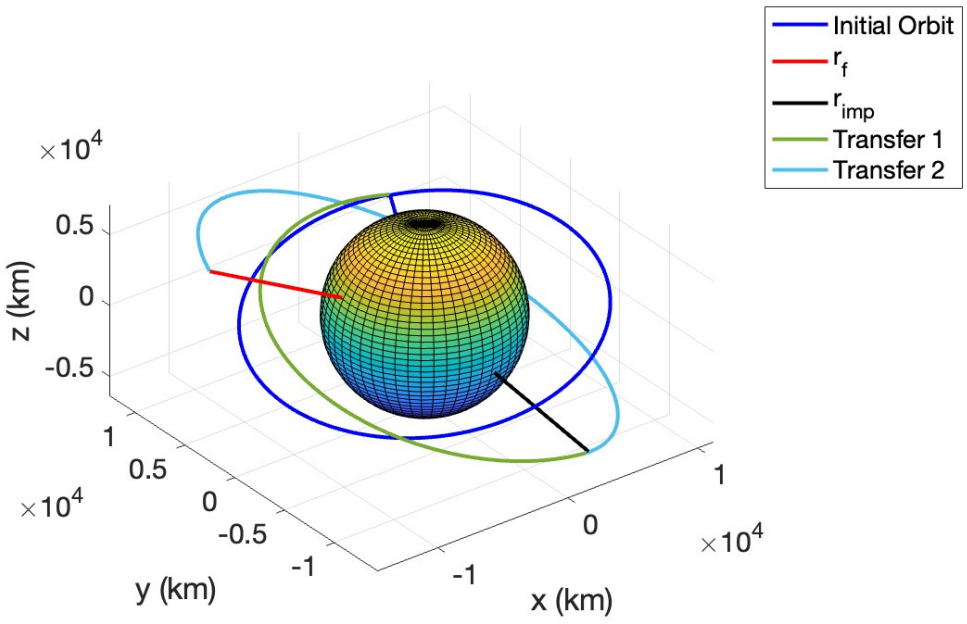

Figure 4-25: Time-Constrained Multi-Impulse Lambert Solution

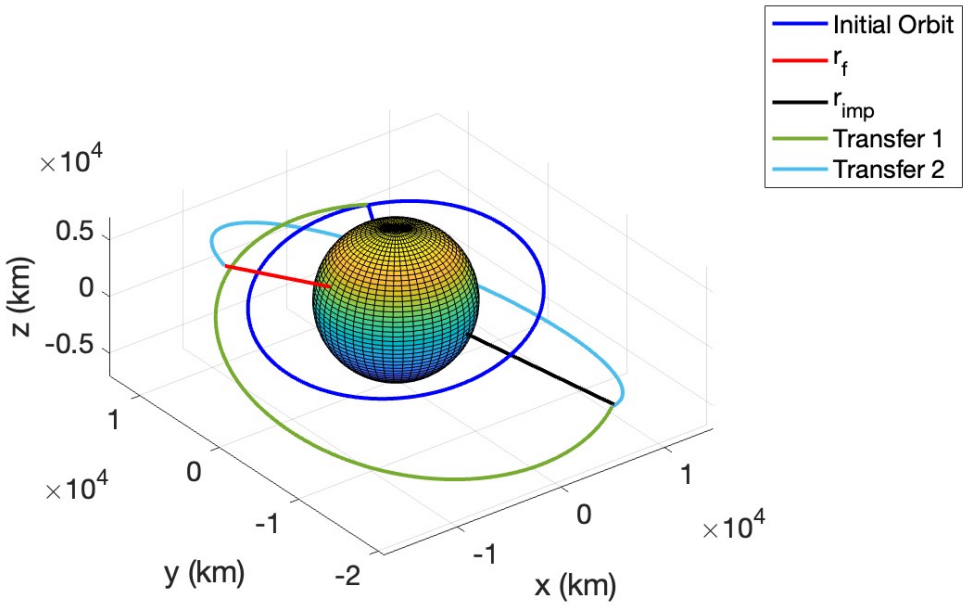

Figure 4-26: Time-Open Multi-Impulse Lambert Solution

take 4,612 s. Hence, the multi-impulse solution provides a more fuel efficient transfer than the single-impulse maneuver. All in all, the time-open solution uses less total Δv, and hence is more fuel optimal, than the time-constrained solution. However, the time-constrained solution is faster and hence more time optimal.

4.9 Use Case: Space Debris Explosion

Space debris is a growing problem for space operations and active debris removal is an active area of research [68]. Explosions of satellites can lead to collisions between space debris fragments and active satellites [33]. Hence, it is of interest to use the KO solution to Lambert's problem to study the potential trajectories of an explosion event that may cause debris to intersect with a satellite's orbit.

An initial circular orbit is assumed for the active satellite. The explosion of another

satellite on a different circular orbit occurs at,

$$\begin{aligned} \mathbf{r}_{ex} &= [7000,\ \ 12,000,\ \ 5000] \text{ km} \\ \mathbf{v}_{ex} &= [-4.30,\ \ 1.46,\ \ 2.52] \text{ km/s} \end{aligned} \tag{4.14}$$

where $\mathbf{v}_{ex}$ is the velocity of the satellite that explodes at $\mathbf{r}_{ex}$. The KO solution to Lambert's problem is used to calculated what Δv must the explosion impart onto its fragments in order to cause a collision with the active satellite in orbit. The period of the active satellite is used as the time constraint. The orbit of the active satellite is discretized by true anomaly into 1 degree segments and the required Δv of the explosion to reach each segment in the corresponding time constraint is calculated. Debris pieces that would crash into the Earth before reaching the orbit of the active satellite are not considered. Furthermore, all trajectories of the debris fragments are prograde. While this assumption constrains the potential number of collisions, it is justified given the initial prograde trajectory of the exploding satellite. Any debris fragment aiming to shift into a retrograde trajectory would have to counterbalance this initial velocity, making it a less likely occurrence. The minimum Δv required to cause a collision is found to be 2.497 km/s and the maximum is 8.894 km/s. The trajectories of the debris that would cause a collision with the active satellite are shown in Figure 4-27. In conclusion, the KO solution to Lambert's problem may be used to help identify possible collisions with space debris and hence aid in collision avoidance maneuver planning.

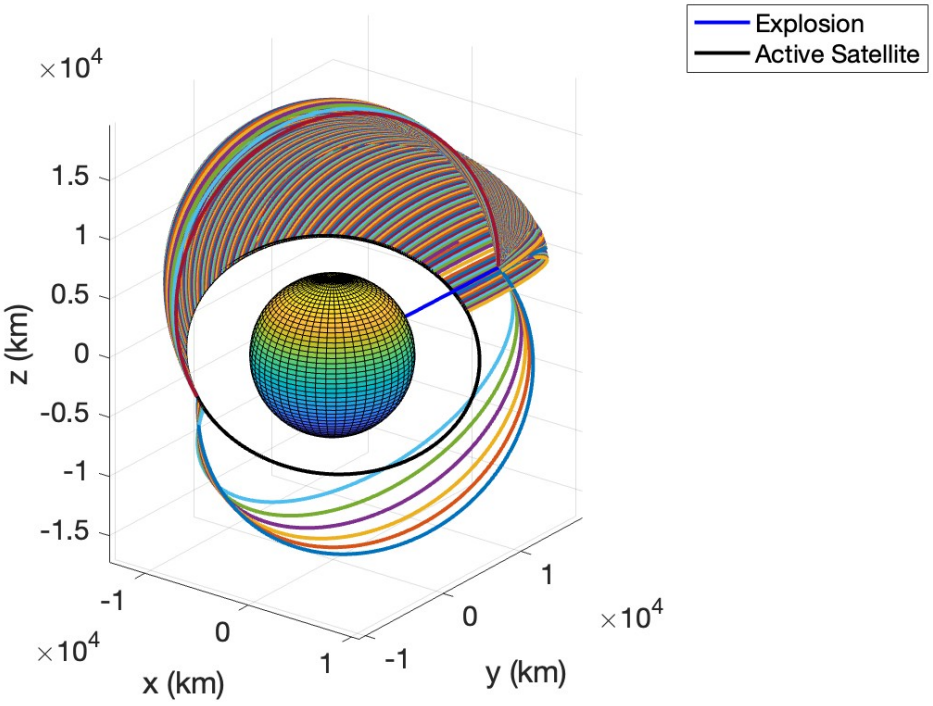

Figure 4-27: Space Debris Explosion

Chapter 5

Spectral Behavior

5.1 Introduction

This chapter studies the spectral behavior of the dynamical systems in which Lambert's problem was solved in previous parts of this Thesis. The Spectral behavior of a dynamical system can provide insights into the stability of the system as well as into its long-term behavior. Studying the spectral behavior can identify natural frequencies and resonances of the system. Furthermore, studying the spectral behavior of both the unperturbed and perturbed dynamical systems of Earth's gravitational field can help in understanding the effects of considering J_2 perturbations on the stability of the solutions.

First, Section 5.2 studies the distribution of the eigenvalues of the Koopman Operator for both the perturbed and unperturbed systems for different orders in the Koopman basis functions. Then, Section 5.3 studies the magnitudes of the Koopman modes for different orders in the basis functions and explains their relation to the accuracy of the solutions presented.

5.2 Koopman Operator Eigenvalues

Studying the spectral behavior of the transfer orbits solved for in Chapter 4 is beneficial as it provides a deeper understanding of the dynamical systems' behaviors [49]

[23]. The eigenvalues of the dynamical system are independent of the initial conditions of the problem since the Koopman matrix is independent of these.

The distribution of eigenvalues of the unperturbed system is shown in Figure 5-1 a) using a set of basis functions of order 3. The real part of these eigenvalues is negligible as it is $O(10^{-15})$. Hence, these eigenvalues are located on the imaginary axis, indicating the dynamical system has oscillatory behavior. The distribution of eigenvalues of the perturbed system is shown in Figure 5-1 b) using the same order for the set of basis functions. The real part of the eigenvalues is no longer negligible, $O(10^{-3})$. This change in behavior of the eigenvalues indicates that the zonal perturbations are affecting the stability and long-term behavior of the system. Generally, these effects render the system more unstable.

The maximum frequency of the eigenvalues increases with an increase in the order of the basis functions used. This increase in maximum frequency comes as a result of the basis functions being computed as a combination of the initial set of variables. Furthermore, the maximum frequency matches the order of the basis functions used. To see this, let ϕ_1 and ϕ_2 be two eigenfunctions of the KO matrix with eigenvalues λ_1 and λ_2,

$$\begin{aligned} \frac{d\phi_1}{dt} &= \lambda_1 \phi_1 \\ \frac{d\phi_2}{dt} &= \lambda_2 \phi_2 \end{aligned} \tag{5.1}$$

Multiplying these two eigenfunctions leads to a third eigenfunction of the system, $g = \phi_1 \phi_2$ with eigenvalue $\lambda_1 + \lambda_2$ [4],

$$\frac{dg}{dt} = \frac{d\phi_1}{dt}\phi_2 + \phi_1 \frac{d\phi_2}{dt} = \lambda_1 \phi_1 \phi_2 + \lambda_2 \phi_1 \phi_2 = (\lambda_1 + \lambda_2)\, g \tag{5.2}$$

An increase in the number of basis functions used corresponds to an increase in the number of eigenfunctions which leads to an increase in the maximum frequency.

The distribution of eigenvalues of the perturbed system with order 7 in the basis functions is shown in Figure 5-2. The maximum value of the imaginary part of the KO eigenvalues is 7. The distribution of eigenvalues of the system for the solution that uses order 9 in the basis functions is shown in Figure 5-3. In this figure, the maximum

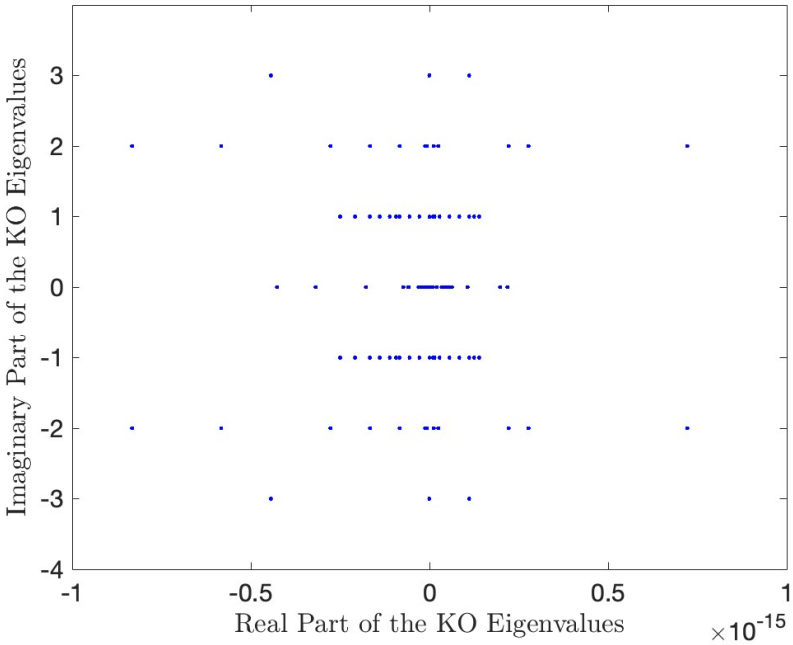

(a) Unperturbed System

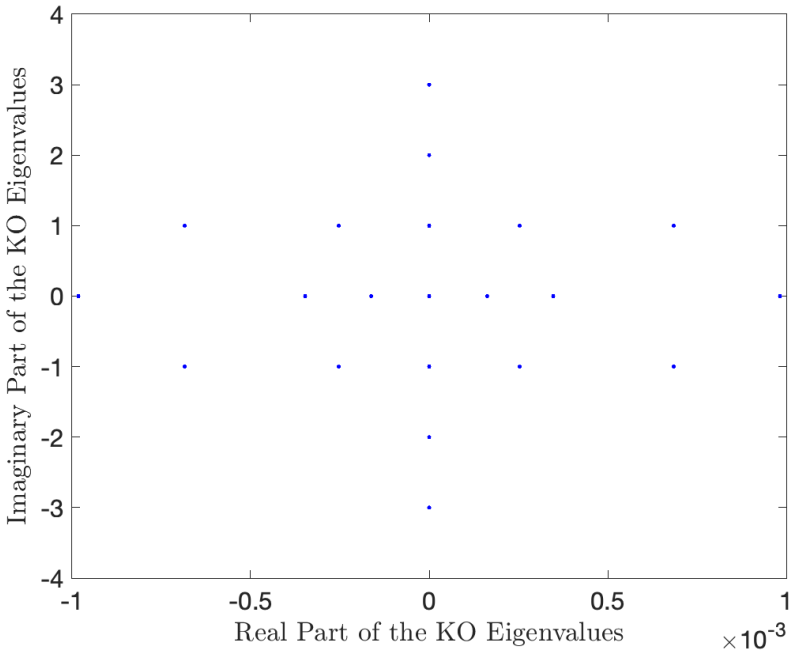

(b) Perturbed System

Figure 5-1: Distribution of Eigenvalues for 3rd Order in Basis Functions

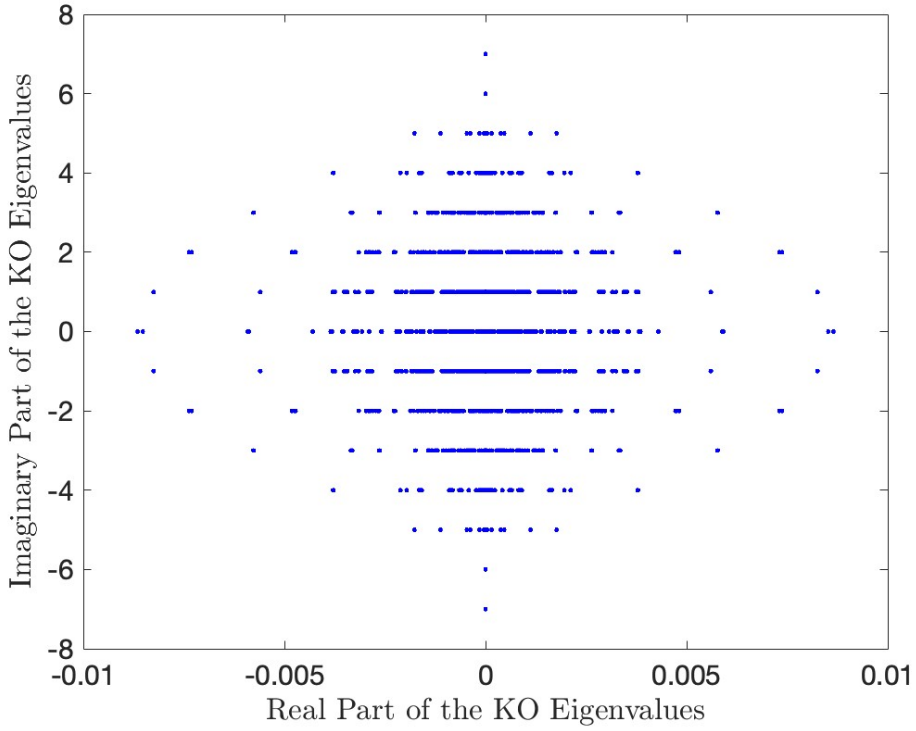

Figure 5-2: Distribution of Eigenvalues for 7th Order in Basis Functions for the Perturbed Dynamical System

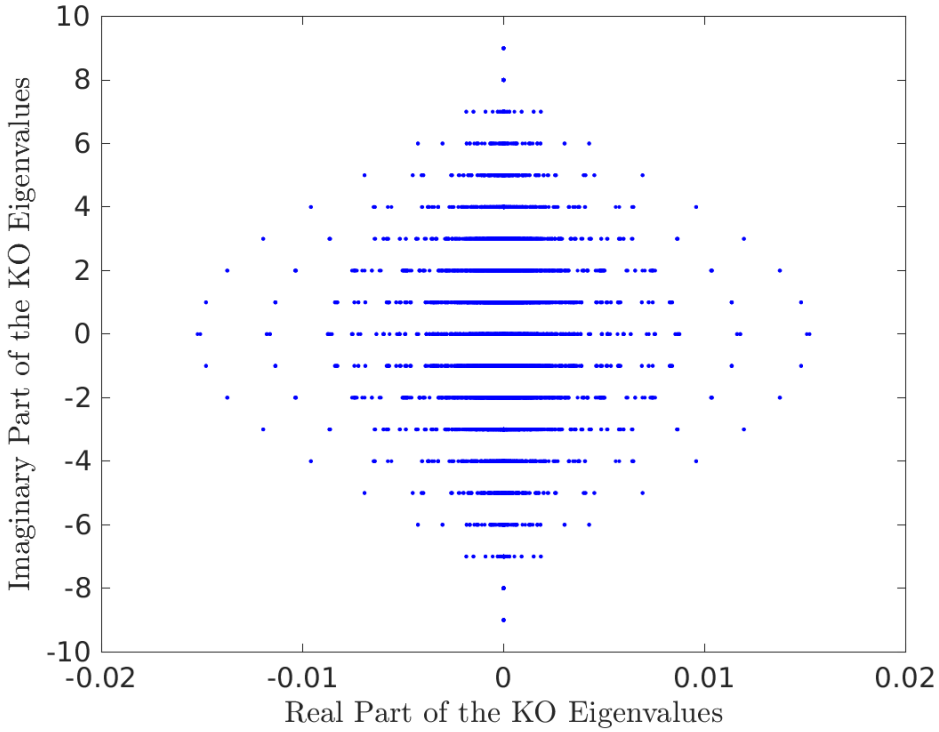

Figure 5-3: Distribution of Eigenvalues for 9th Order in Basis Functions for the Perturbed Dynamical System

value of the imaginary part of the KO eigenvalues is 9. Hence, the eigenvalues in Figure 5-3 do not exactly match up with those of Figure 5-2 because of the increase in the basis functions used which increases the total number of eigenvalues. Furthermore, the position of the repeated eigenvalues between the two Figures varies slightly due to the fact that increasing the order of the basis functions increases the accuracy of the solution by increasing the accuracy of the eigenvalues. However, the overall shape and location of the eigenvalues is kept in both Figures. Hence, the overall spectral decomposition of the dynamics remains, however, it becomes more accurate as the order is increased which increases the number of eigenvalues that are farther from the origin. This eigenvalue distribution is representative of the whole J_2 dynamical system for any initial conditions that are considered for solving Lambert's problem since the Koopman Matrix is independent of these conditions.

5.3 Koopman Mode Magnitudes

To better understand how the solution to Lambert's problem in the perturbed system depends on each Koopman mode, the Koopman mode magnitudes are plotted against the absolute values of the Koopman eigenvalues. The magnitudes are plotted for orders 7, 8, and 9 in the KO basis functions in Figure 5-4. The number of modes increases with an increase in order, however the magnitudes of these modes decrease in value. Hence, increasing the order of the KO basis functions still leads to an increase in the accuracy of the solution since influential modes are being added. However, as the order is increased, the benefits to improving the accuracy of the solution decreases. When using higher-order basis functions, there exists a trade-off between the increase in computational complexity and the improvement in the accuracy of the solution. As explained in Section 4.2.2, when solving for the solutions to Lambert's problem in the perturbed system, order 7 in the basis functions is used as this order is able to capture the non-linearities of the system. As can be seen from Figure 5-4, higher orders than 7 have diminishing returns on improving the accuracy of the solutions.

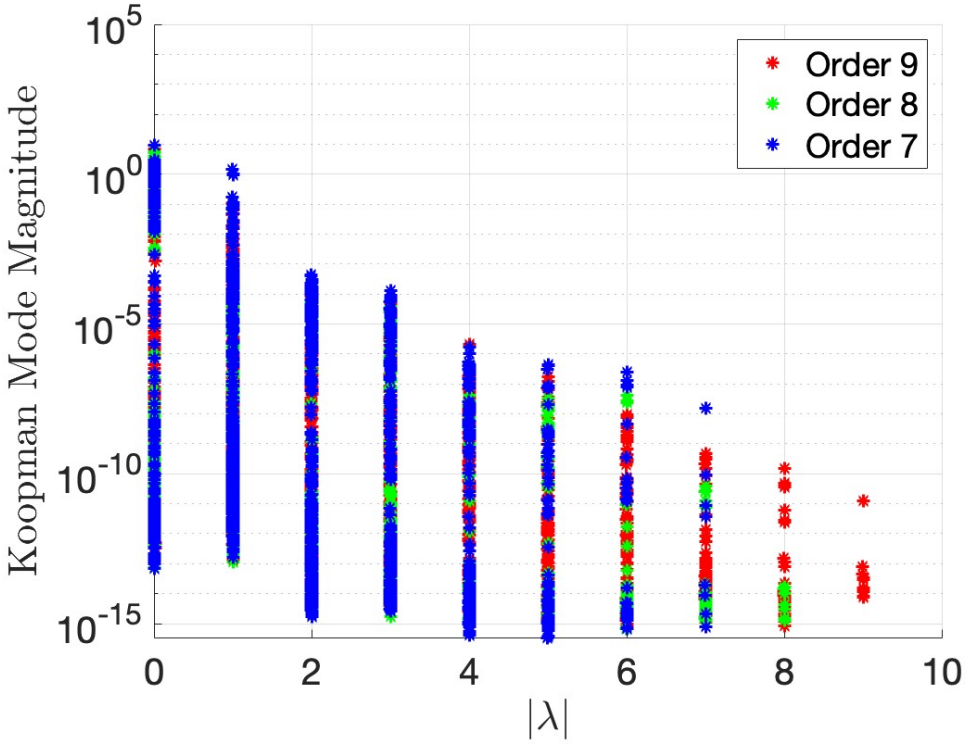

Figure 5-4: Koopman Mode Magnitudes

Chapter 6

Conclusion

6.1 Thesis Summary

This Thesis addresses the study of applying an operator theoretic approach to solving nonlinear problems in astrodynamics by applying the Koopman Operator to solving Lambert's problem. The first chapter introduces a general motivation for studying nonlinear problems in astrodynamics using an operator theoretic approach. In particular, a motivation to study Lambert's problem using the Koopman Operator is given. A summary of the relevant literature is introduced on both the Koopman Operator and Lambert's problem. The main contributions of these related studies are discussed. Then, the specific objectives of the Thesis are identified including a motivation to study the spectral behaviors of the dynamical systems via the Koopman Operator.

Chapter 2 gives the essential theoretical background of the Koopman Operator and associated mathematical methods. It starts by introducing the Koopman Operator formulation, outlining the major benefits attainable through its application to nonlinear systems. Then the chapter overviews the computation of the Koopman eigenfunctions with an introduction to the Galerkin method. After introducing the calculation of the Koopman matrix, the evolution of the basis functions is described. As part of the final section, the evolution of the observables is provided which is used throughout the rest of the Thesis.

The third chapter defines Lambert's problem and introduces key algorithms needed in its solution. After giving an overview of the standard formulation of Lambert's problem with a time constraint, the chapter overviews variants of Lambert's problem including the multiple revolutions solution, the minimum energy solution, the minimum Δv solution, and the multi-impulse solution. An algorithm to solve Lambert's problem using Lagrange coefficients is introduced. This algorithm is used throughout the rest of the Thesis to compare against the Koopman Operator solutions. Furthermore, the Levenberg-Marquadt algorithm used in the Koopman Operator solution is outlined. The final section of the chapter presents the orbital elements that gives the linearization needed for the Koopman Operator approach.

Next, Chapter 4 presents the results of applying the Koopman Operator to solve Lambert's problem in both the unperturbed system and perturbed system. Single-revolution solutions are presented and compared against another Lambert solver. Then a variety of different initial conditions are considered including transfers to a highly eccentric orbit, to an orbit at the critical inclination and to a geostationary orbit. The errors of each solution are also presented. The minimum energy and minimum Δv solutions are solved using the Koopman Operator approach. Furthermore, efficient trajectories are mapped using pork-chop plots. Comparisons with numerical methods are made. Then, multiple revolution solutions to Lambert's problem solved using the Koopman Operator approach are presented, followed by an error-correcting method and the multi-impulse solution. Finally, the last section applies the Koopman Operator solution to the use case of mapping space debris collisions from an explosion. The chapter highlights the applicability of the Koopman Operator method.

Lastly, Chapter 5 presents a spectral behavior analysis of the dynamical systems studied in this Thesis, particularly the unperturbed and perturbed dynamical systems. The Koopman Operator eigenvalue distributions are presented for various orders of the Koopman basis functions. The second section focuses on the influence on accuracy that the magnitudes of the Koopman modes have for various orders in the basis functions. A more profound insight into the spectral behavior of the dynamical systems is offered.

6.2 Main Findings

The main objective of this Thesis has been to present the benefits of using an operator theoretic approach to solving nonlinear problems in astrodynamics by introducing a solution to Lambert's problem using the Koopman Operator. Many variations of Lambert's problem were solved, showing the wide range of applicability of the method. Furthermore, comparisons with numerical methods and other solvers throughout the Thesis have shown the robustness and accuracy of the Koopman Operator approach.

First, the Koopman Operator solution presents advantages in terms of computational efficiency. The Koopman Operator matrix needs only to be calculated once for any dynamical system. Hence, in this Thesis the Koopman Operator matrix was calculated once for the unperturbed dynamical system and once for the perturbed dynamical system for each specified order of the basis functions. The appropriate Koopman Operator matrix was used to solve variations of Lambert's problem for a variety of initial conditions. In the single revolution solution, the solutions found using the Koopman Operator outperformed those found using the algorithm by Bate, Muller and White, and Bond and Allman by bringing the satellite closer to its desired position in the perturbed dynamical system. However, the BMW algorithm outperformed the Koopman Operator method when solving Lambert's problem in the unperturbed case. The Koopman Operator solution was also compared to numerical integration of the J_2 dynamical system. A decrease in the error of the solution was attained with an increase in the order of the Koopman basis functions. An error of about 70 cm was attained for order 7 in the basis functions, 4 orders of magnitude smaller than the error attained for order 3 in the basis functions.

Next, a variety of initial conditions were considered and transfer orbits were found. These included transfers to a highly eccentric orbit, to an orbit at the critical inclination, and to a geostationary equatorial orbit. The transfer to the critical inclination had the smallest error between the Koopman Operator solution and that of the numerical propagation while the transfer to GEO had the largest error. The minimum energy and minimum Δv transfers were solved for. These solutions are important for

efficient resource use and fuel consumption, a critical aspect in mission planning and success. Furthermore, efficient trajectories were found using pork-chop plots and the departure and arrival orbital positions that correspond to the global minimum Δv were identified. Any reduction in the required Δv from using such transfers directly translates to cost savings, longer mission durations, and expanded mission capabilities. A comparison with a numerical method showed the mean relative error of the Koopman Operator solution to be 0.339%.

A multitude of multiple revolutions solutions were solved for, giving possible solutions for a variety of time constraints corresponding to different semi-major axes. The specific energy and total Δv's of these solutions decreased as the number of revolutions increased. An error-correcting method was introduced that recalculated the optimal transfer orbit during the transfer and reduced the difference between the desired final position and the attained final position by an order in magnitude from 7.56 km to 0.88km. Furthermore, the optimal position for a multi-impulse solution was found for a satellite on a transfer orbit in the perturbed dynamical system with two impulse maneuvers. A use case regarding the application of the Koopman Operator to tracking collisions from a space debris explosion highlighted the range of applicability of the method.

The spectral behaviors of the unperturbed and perturbed dynamical systems were provided, giving a deeper understanding of these systems' dynamics. The stability of the systems were discussed. The maximum frequency of the eigenvalues of the Koopman Operator were shown to increase with the order of the basis functions used. This increase corresponds to an increase in accuracy of the solutions as could be seen in Chapter 4. By plotting the Koopman modes as a function of the absolute value of the eigenvalue frequencies, the diminishing returns on improving the accuracy of the solutions by increasing the order of the basis functions were demonstrated.

Overall, the Koopman Operator presents a unique advantage in the calculation of solutions to Lambert's problem as it provides a method to linearize the high-dimensional nonlinear dynamical systems this problem is defined in. This linearization makes the computations more tractable and efficient. Moreover, the Koopman

Operator's ability to handle complex, multi-variable systems such as the J_2 perturbed system, makes it an excellent tool to solve nonlinear problems in astrodynamics.

6.3 Future Work

Based on the results of applying the Koopman Operator to solving Lambert's problem in this Thesis, various directions of future research paths are identified:

- Consider more applications of operator theory to solving nonlinear problems in astrodynamics. In particular, applying the Koopman Operator to linearize cis-lunar dynamics, using the Koopman Operator to solve the low-thrust trajectory optimization problem while taking into account J_2 perturbations, and using the Koopman Operator to solve for optimal orbit trajectories while taking into account perturbations other than J_2 perturbations such as the effects of solar radiation pressure and atmospheric drag.

- Explore ways to decrease the computational complexity involved in using very high orders of basis functions of the Koopman Operator. Orders upwards of 30 could significantly decrease the errors involved in using the Koopman Operator, however, such orders beyond 11 involve a large matrix calculation that becomes computationally infeasible. The implementation of order 7 of the basis functions in this Thesis resulted in decreasing the error of the solutions by 4 orders of magnitude compared to an implementation of order 3 of the basis functions. Further increasing the order would inevitably decrease the error significantly. Furthermore, solving nonlinear problems in more complex systems would benefit from having higher orders calculated with less complexity as their nonlinearities would be captured better using such higher orders. This research direction could also help improve the accuracy of the Koopman Operator solution for long time constraints.

- Consider using a data-driven approach that uses dynamic mode decomposition to approximate the Koopman Operator with a best-fit linear model. This type

of approach would allow for a verification of the geometric approach employed in this Thesis. It would also allow for a verification of the accuracy of the equations used in this Thesis to represent the orbital elements of the dynamical systems. Furthermore, employing a data-driven approach would increase the range of applicability of the Koopman Operator to other nonlinear problems since a polynomial representation of the system under study can be difficult to find.

Appendix A

Additional Figures

A.1 Time-θ Conversion

The propagation of time and that of the time regularization derived from Equation 3.14 with respect to θ for one revolution of a random orbit.

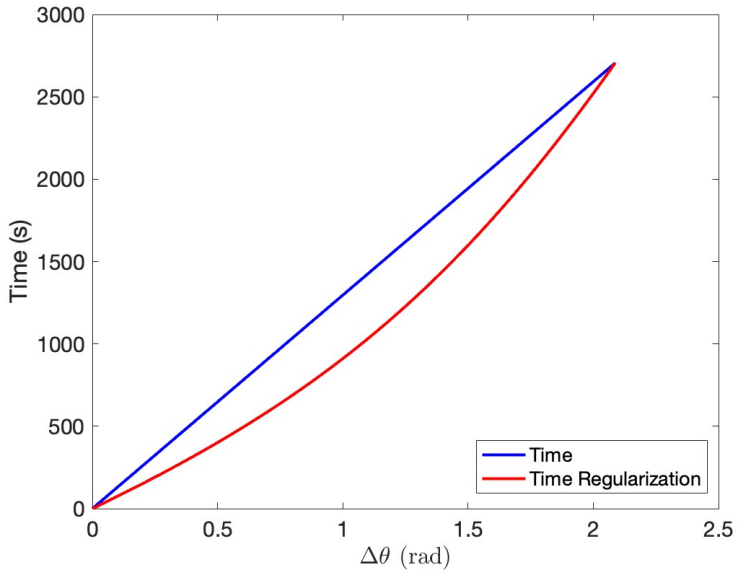

Figure A-1: Time-θ Conversion

Bibliography

[1] Prasad V. Arlulkar and Smita D. Naik. Solution Based on Dynamical Approach for Multiple-Revolution Lambert Problem. *Journal of Guidance Control and Dynamics*, 34:920–923, 2011.

[2] David Arnas. Solving Ordinary Differential Equations Using Schur Decomposition, 2021.

[3] David Arnas and Richard Linares. A Set of Orbital Elements to Fully Represent the Zonal Harmonics Around an Oblate Celestial Body. *Monthly Notices of the Royal Astronomical Society*, 502(3):4247–4261, 01 2021.

[4] David Arnas and Richard Linares. Approximate Analytical Solution to the Zonal Harmonics Problem Using Koopman Operator Theory. *Journal of Guidance, Control, and Dynamics*, 44:1–15, 08 2021.

[5] Nitin Arora and Ryan Russell. A Fast and Robust Multiple Revolution Lambert Algorithm using a Cosine Transformation. *Advances in the Astronautical Sciences*, 150:411–430, 01 2014.

[6] Giulio Avanzini. A Simple Lambert Algorithm. *Journal of Guidance, Control, and Dynamics*, 31(6):1587–1594, 2008.

[7] Martín Avendaño and Daniele Mortari. A Closed-Form Solution to the Minimum ΔV_{tot}^2 Lambert's Problem. *Celestial Mechanics and Dynamical Astronomy*, 106, 01 2009.

[8] Roger R. Bate, Donald Mueller, and Jerry White. *Fundamentals of astrodynamics*. Dover Publications, Inc., Mineola, New York, revised and updated second edition. edition, 2020.

[9] Richard H. Battin and Robin M. Vaughan. An Elegant Lambert Algorithm. *Journal of Guidance Control and Dynamics*, 7:662–670, 1983.

[10] J. Benkhoff, J Benkhoff, G Murakami, W Baumjohann, S Besse, E Bunce, M Casale, G Cremosese, K-H Glassmeier, H Hayakawa, D Heyner, H Hiesinger, J Huovelin, H Hussmann, V Iafolla, L Iess, Y Kasaba, M Kobayashi, A Milillo, and I G Mitrofanov. BepiColombo - Mission Overview and Science Goals. *Space science reviews.*, 217(8):90–, 2021-12.

[11] Antonio Fernando Bertachini de Almeida Prado and Roger A. Broucke. The Minimum Delta-V Lambert's Problem. Conference held in Santos, Brazil, 21-25 Nov. 1994, January 1994.

[12] Robert Blanchard and E. R. Lancaster. *A Unified Form of Lambert's Theorem.* NASA, 1968.

[13] Frederick W. Boltz. Second-Order p-Iterative Solution of the Lambert/Gauss Problem. *Journal of the Astronautical Sciences*, 32:475–485, December 1984.

[14] Victor R. Bond. *An Analytical Singularity-Free Solution to the J2 Perturbation Problem.* NASA, Legacy CDMS, 1979.

[15] Victor R. Bond and Mark C. Allman. *Modern astrodynamics : fundamentals and perturbation methods.* Princeton University Press, Princeton, N.J, 1996.

[16] Karl Bopp. Leonhard Eulers und Johann Heinrich Lamberts Briefwechsel. *Abh. Preuß. Akad. Wiss., Phys.-Math. Kl.*, 1924:45 s., 1924.

[17] Thomas A. A. Broadbent. Theory of the Motion of Heavenly Bodies. By K. F Gauss. Pp. xvii, 326, 40. 24s. 1857; reprinted 1964. (Dover.). *Mathematical gazette*, 48(365):352–352, 1964.

[18] Steven L. Brunton, Marko Budišić, Eurika Kaiser, and J. Nathan Kutz. Modern Koopman Theory for Dynamical Systems, 2021.

[19] Richard L. Burden. *Numerical analysis.* Cengage Learning, Boston, MA, tenth edition. edition, 2016.

[20] Maria L. Castano, Andrew Hess, Giorgos Mamakoukas, Tong Gao, Todd Murphey, and Xiaobo Tan. Control-oriented Modeling of Soft Robotic Swimmer with Koopman Operators. *2020 IEEE/ASME International Conference on Advanced Intelligent Mechatronics (AIM)*, 2020.

[21] Ti Chen and Jinjun Shan. Koopman-Operator-Based Attitude Dynamics and Control on SO(3). *Journal of Guidance, Control, and Dynamics*, 43(11):2112–2126, 2020.

[22] Tong Chen, E. van Kampen, H. Yu, and Q. P. Chu. Optimization of Time-Open Constrained Lambert Rendezvous Using Interval Analysis. *Journal of Guidance, Control, and Dynamics*, 36(1):175–184, 2013.

[23] Nelida Crnjaric-Zic, Senka Macesic, and Igor Mezic. Koopman Operator Spectrum for Random Dynamical Systems, 2019.

[24] Howard Curtis. *Orbital Mechanics for Engineering Students.* Elsevier Aerospace Engineering Series. Elsevier Science and Technology, San Diego, 2009.

[25] David de la Torre Sangrà and Elena Fantino. Review of Lambert's Problem, 2021.

[26] J. R. Doll and Frank W. Gobetz. A Survey of Impulsive Trajectories. *AIAA Journal*, 7:801–834, 1969.

[27] R. C. Engels and John L. Junkins. The Gravity-Perturbed Lambert Problem - a KS Variation of Parameters Approach. *Celestial Mechanics*, 24(1):3–21, May 1981.

[28] Curtis F. Gerald. *Applied numerical analysis*. Pearson/Addison-Wesley, Boston, 7th ed. edition, 2004.

[29] Philip E. Gill. *Practical Optimization* . Classics in applied mathematics ; 81. Society for Industrial and Applied Mathematics SIAM, 3600 Market Street, Floor 6, Philadelphia, PA 19104, Philadelphia, Pennsylvania, 2019.

[30] R. H. Gooding. A Procedure for the Solution of Lambert's Orbital Boundary-Value Problem. *Celestial Mechanics and Dynamical Astronomy*, 48(2):145–165, June 1990.

[31] David J. Griffiths. *Introduction to Quantum Mechanics* . Cambridge University Press, Cambridge, United Kingdom, third edition. edition, 2018 - 2018.

[32] John Guckenheimer and Philip Holmes. *Nonlinear Oscillations, Dynamical Systems, and Bifurcations of Vector Fields*, volume 42 of *Applied Mathematical Sciences*. Springer, New York, NY, 1983.

[33] Ryusuke Harada, Satomi Kawamoto, Nobuaki Nagaoka, and Toshiya Hanada. The Impact Assessment of Accidental Explosions of Large Constellations on Low Earth Orbit Environment. *Journal of Space Safety Engineering*, 2023.

[34] Quan He, Jian Li, and Chao Han. Multiple-Revolution Solutions of the Transverse-Eccentricity-Based Lambert Problem. *Journal of Guidance, Control, and Dynamics*, 33(1):265–269, 2010.

[35] Christian Hofmann, Simone Servadio, Richard Linares, and Francesco Topputo. Advances in Koopman Operator Theory for Optimal Control Problems in Space Flight. In *2022 AAS/AIAA Astrodynamics Specialist Conference*. AAS/AIAA, 08 2022.

[36] Dario Izzo. Revisiting Lambert's Problem. *Celestial Mechanics and Dynamical Astronomy*, 03 2014.

[37] Donald J. Jezewski. K/S Two-Point-Boundary-Value Problems. *Celestial Mechanics*, 14(1):105–111, August 1976.

[38] Donald J. Jezewski. A Noncanonical Analytic Solution to the J $_2$ Perturbed Two-body Problem. *Celestial Mechanics*, 30(4):343–361, August 1983.

[39] John L. Junkins and Puneet Singla. How Nonlinear Is It? A Tutorial on Nonlinearity of Orbit and Attitude Dynamics. *The Journal of the astronautical sciences*, 52(1-2):7–60, 2004.

[40] Bernard. O. Koopman. Hamiltonian Systems and Transformation in Hilbert Space. *Proceedings of the National Academy of Sciences*, 17(5):315–318, 1931.

[41] J. Kriz. A Uniform Solution of the Lambert Problem. *Celestial Mechanics*, 14(4):509–513, December 1976.

[42] Joseph Louis Lagrange. *Mécanique Analytique* . Cambridge library collection. Cambridge University Press, Cambridge ;, 2009 - 1811.

[43] Henzeh Leeghim and Belgacem A. Jaroux. Energy-Optimal Solution to the Lambert Problem. *Journal of Guidance, Control, and Dynamics*, 33(3):1008–1010, 2010.

[44] Richard Linares. Koopman Operator Theory Applied to The Motion of Satellites. In *2019 AAS/AIAA Astrodynamics Specialist Conference*, 08 2019.

[45] Laura Ann Loechler. An Elegant Lambert Algorithm for Multiple Revolution Orbits. Master's thesis, Massachusetts Institute of Technology, 1988.

[46] Di Luo, Jiayu Shen, Rumen Dangovski, and Marin Soljačić. Koopman Operator Learning for Accelerating Quantum Optimization and Machine Learning. In *APS March Meeting 2023*. APS, 11 2022.

[47] Qinqin Luo, Zhanfeng Meng, and Chao Han. Solution Algorithm of a Quasi-Lambert's Problem with Fixed Flight-Direction Angle Constraint. *Celestial Mechanics and Dynamical Astronomy*, 109:409–427, 04 2011.

[48] Igor Mezic. Analysis of Fluid Flows via Spectral Properties of the Koopman Operator. *Annual Review of Fluid Mechanics*, 45:357–378, 01 2013.

[49] Igor Mezic. Spectrum of the Koopman Operator, Spectral Expansions in Functional Spaces, and State-Space Geometry. *Journal of Nonlinear Science*, 30, 10 2020.

[50] Samuel Otto and Clarence Rowley. Koopman Operators for Estimation and Control of Dynamical Systems. *Annual Review of Control Robotics and Autonomous Systems*, 4, 02 2021.

[51] John E. Prussing. A Class of Optimal Two-Impulse Rendezvous Using Multiple-Revolution Lambert Solutions. *Journal of The Astronautical Sciences*, 48:131–148, 2000.

[52] Marco B. Quadrelli, Lincoln J. Wood, Joseph E. Riedel, Michael C. McHenry, MiMi Aung, Laureano A. Cangahuala, Richard A. Volpe, Patricia M. Beauchamp, and James A. Cutts. Guidance, Navigation, and Control Technology Assessment for Future Planetary Science Missions. *Journal of guidance, control, and dynamics*, 38(7):1165–1186, 2015.

[53] Gerald W. Recktenwald. *Numerical methods with MATLAB : implementations and applications*. Prentice Hall, Upper Saddle River, N.J, 2000.

[54] G. Scheifele and O. Graf. Analytical Satellite Theories Based on a New Set of Canonical Elements. In *Mechanics and Control of Flight Conference*. AAS/AIAA, 1974.

[55] Walkiria Schulz and Antonio Prado. Optimal Space Maneuvers in Three Dimensions. *Journal of The Brazilian Society of Mechanical Sciences and Engineering - J BRAZ SOC MECH SCI ENG*, 28, 10 2006.

[56] Andrey B. Sergeyevsky, Gerald C. Snyder, and Ross A. Cunniff. *Interplanetary Mission Design Handbook. Volume 1, part 2: Earth to Mars Ballistic Mission Opportunities, 1990-2005*. NASA, Legacy CDMS, 1983.

[57] Simone Servadio, David Arnas, and Richard Linares. A Koopman Operator Tutorial with Othogonal Polynomials, 2022.

[58] Simone Servadio, David Arnas, and Richard Linares. Dynamics Near the Three-Body Libration Points via Koopman Operator Theory. *Journal of Guidance, Control, and Dynamics*, 45(10):1800–1814, 2022.

[59] Haijun Shen and Panagiotis Tsiotras. Using Battin's Method To Obtain Multiple-Revolution Lambert's Solutions. In *2003 AAS/AIAA Astrodynamics Specialist Conference*. AAS/AIAA, 08 2003.

[60] Gregory Snyder and Zhuoyuan Song. Koopman Operator Theory for Nonlinear Dynamic Modeling using Dynamic Mode Decomposition, 2021.

[61] Victor G. Szebehely. *Analysis of the Orbital Transfer Problem in Three-Dimensional Space*, pages 627–654. Academic Press, 1964.

[62] Naoya Takeishi, Yoshinobu Kawahara, and Takehisa Yairi. Learning Koopman Invariant Subspaces for Dynamic Mode Decomposition. In I. Guyon, U. Von Luxburg, S. Bengio, H. Wallach, R. Fergus, S. Vishwanathan, and R. Garnett, editors, *Advances in Neural Information Processing Systems*, volume 30. Curran Associates, Inc., 2017.

[63] Blair Thompson. Enhancing Lambert Targeting Methods to Accommodate 180-Degree Orbital Transfers. *Journal of Guidance, Control, and Dynamics*, 34:1925–1929, 11 2011.

[64] James Dana Thorne. Series Reversion/Inversion of Lambert's Time Function. Master's thesis, Wright-Patterson Air Force Base, Ohio, December 1989.

[65] John v. Neumann. Zur Operatorenmethode In Der Klassischen Mechanik. *Annals of Mathematics*, 33(3):587–642, 1932.

[66] Sébastien E. Wailliez. On Lambert's Problem and the Elliptic Time of Flight Equation: A Simple Semi-Analytical Inversion Method. *Advances in Space Research*, 53(5):890–898, 2014.

[67] Changxuan Wen, Yushan Zhao, and Peng Shi. Derivative Analysis and Algorithm Modification of Transverse-Eccentricity-Based Lambert Problem. *Journal of Guidance, Control, and Dynamics*, 37(4):1195–1201, 2014.

[68] K. Wormnes, Ronan Le Letty, Leopold Summerer, R. Schonenborg, Olivier Dubois-Matra, E. Luraschi, A. Cropp, H. Krag, and Jessica Delaval. Esa Technologies for Space Debris Remediation. *Proceedings of the 6th IAASS Conference: Safety is Not An Option*, pages 3–4, 01 2013.

[69] Bin Yang, Shuang Li, Jinglang Feng, and Massimiliano Vasile. Fast Solver for J2-Perturbed Lambert Problem Using Deep Neural Network. *Journal of Guidance, Control, and Dynamics*, 45(5):875–884, may 2022.

[70] Gang Zhang, Daniele Mortari, and Di Zhou. Constrained Multiple-Revolution Lambert's Problem. *Journal of Guidance Control and Dynamics*, 33:1779–1786, 2010.